USGS
science for a changing world

Prepared in cooperation with the U.S. Fish and Wildlife Service

Application of the Stream Salmonid Simulator (S3) to the Restoration Reach of the Trinity River, California—Parameterization and Calibration

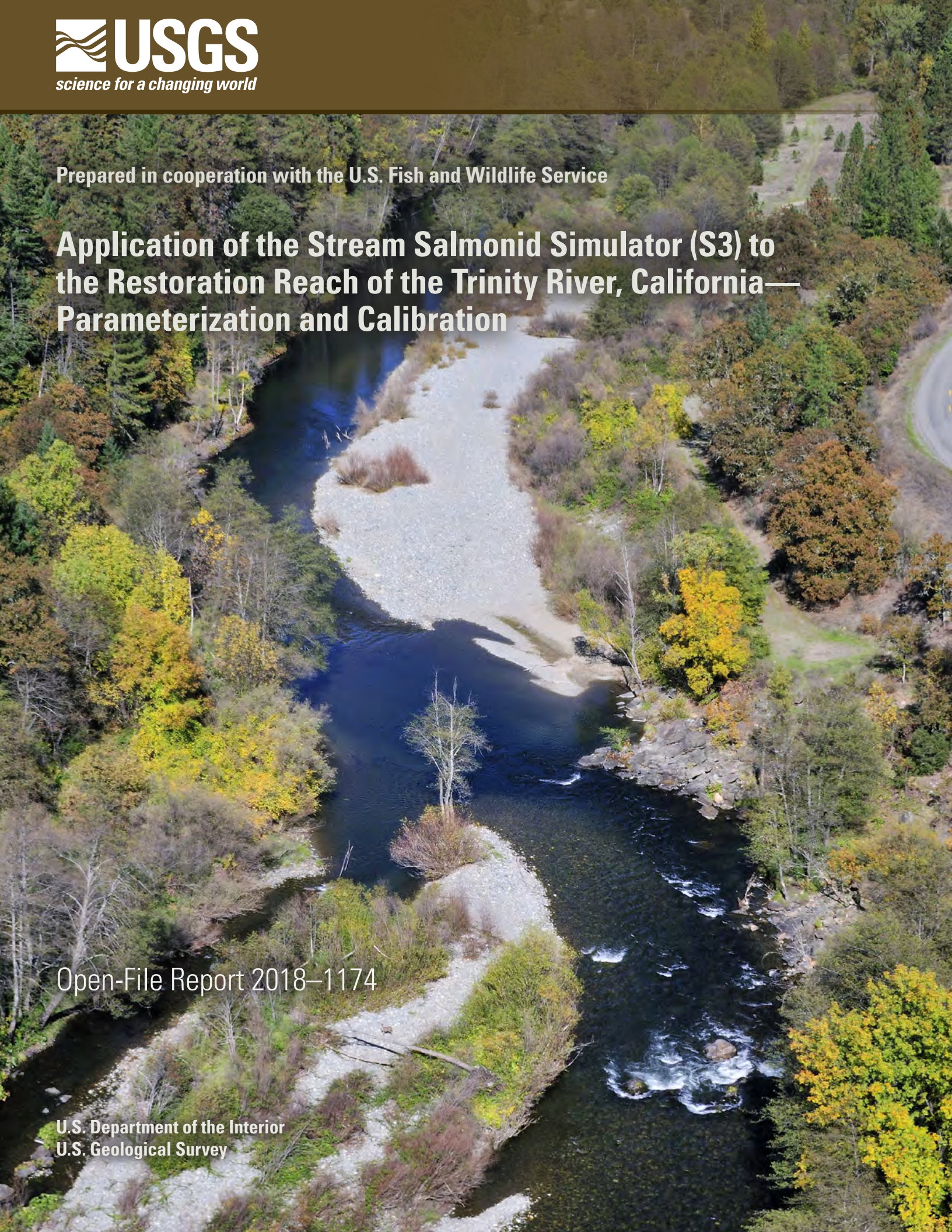

Open-File Report 2018–1174

U.S. Department of the Interior
U.S. Geological Survey

Cover: Trinity River, California, October 18, 2011. Photograph by Kenneth Decamp (used with permission of the Trinity River Restoration River Program).

Application of the Stream Salmonid Simulator (S3) to the Restoration Reach of the Trinity River, California—Parameterization and Calibration

By Russell W. Perry, Edward C. Jones, John M. Plumb, Nicholas A. Som, Nicholas J. Hetrick, Thomas B. Hardy, Joseph C. Polos, Aaron C. Martin, Justin S. Alvarez, and Kyle P. De Juilio

Prepared in cooperation with the U.S. Fish and Wildlife Service

Open-File Report 2018–1174

U.S. Department of the Interior
U.S. Geological Survey

U.S. Department of the Interior
RYAN K. ZINKE, Secretary

U.S. Geological Survey
James F. Reilly II, Director

U.S. Geological Survey, Reston, Virginia: 2018

Suggested citation:
Perry, R.W., Jones, E.C., Plumb, J.M., Som, N.A., Hetrick, N.J., Hardy, T.B., Polos, J.C., Martin, A.C., Alvarez, J.S., and De Juilio, K.P., 2018, Application of the Stream Salmonid Simulator (S3) to the restoration reach of the Trinity River, California—Parameterization and calibration: U.S. Geological Survey Open-File Report 2018-1174, 64 p., https://doi.org/10.3133/ofr20181174.

ISSN 2331-1258 (online)

Contents

Figures

Tables

Conversion Factors

International System of Units to U.S. customary units

Multiply	By	To obtain
	Length	
millimeter (mm)	0.03937	inch (in.)
meter (m)	3.281	foot (ft)
kilometer (km)	0.6214	mile (mi)
	Flow rate	
meter per second (m/s)	3.281	foot per second (ft/s)

U.S. customary units to International System of Units

Multiply	By	To obtain
	Flow rate	
foot per second (ft/s)	0.3048	meter per second (m/s)
cubic foot per second (ft^3/s)	0.02832	cubic meter per second (m^3/s)
	Area	
square foot (ft^2)	0.09290	square meter (m^2)

Temperature in degrees Celsius (°C) may be converted to degrees Fahrenheit (°F) as follows:

$$°F=(1.8×°C)+32$$

Application of the Stream Salmonid Simulator (S3) to the Restoration Reach of the Trinity River, California—Parameterization and Calibration

By Russell W. Perry[1], Edward C. Jones[1], John M. Plumb[1], Nicholas A. Som[2], Nicholas J. Hetrick[2], Thomas B. Hardy[3], Joseph C. Polos[2], Aaron C. Martin[4], Justin S. Alvarez[5], and Kyle P. De Juilio[4]

Executive Summary

In this report, we constructed and parameterized the Stream Salmonid Simulator (S3) for the 64-kilometer "Restoration Reach" of the Trinity River, just downstream of Lewiston Dam in northern California. S3 is a deterministic life-stage-structured population model that tracks daily growth, movement, and survival of juvenile salmon. A key theme of the model is that river flow affects habitat availability and capacity, which in turn drives density-dependent population dynamics. To explicitly link population dynamics to habitat quality and quantity, the river environment is constructed as a one-dimensional series of linked habitat units, each of which has an associated daily timeseries of discharge, water temperature, and useable habitat area or carrying capacity. In turn, the physical characteristics of each habitat unit and the number of fish occupying each unit drive survival and growth within each habitat unit and movement of fish among habitat units.

The physical template of the Restoration Reach was formed by classifying the river into 356 meso-habitat units comprised of runs, riffles, and pools. For each habitat unit, we developed a timeseries of daily flow, water temperature, amount of available spawning habitat, and fry and parr carrying capacity. Capacity timeseries were constructed using state-of-the-art models of spatially explicit hydrodynamics and quantitative fish habitat relationships developed for the Trinity River. These variables were then used to drive population dynamics such as egg growth and survival and juvenile movement, growth, and survival.

We estimated key movement and survival parameters by calibrating the model to five years of weekly juvenile abundance estimates from a rotary screw trap located near the downstream terminus of the Restoration Reach. The calibration consisted of replicating historical conditions as closely as possible (for example, flow; temperature; spawner abundance, spawning location and timing, and hatchery releases), and then running the model to predict weekly abundance passing the trap location. We also evaluated alternative model structures that included either density-independent movement and survival, density-dependent survival, or density-dependent movement. AIC model selection criterion was used to evaluate the strength of evidence for alternative model structures to replicate the observed abundance estimates.

---

[1]U.S. Geological Survey.
[2]U.S. Fish and Wildlife Service.
[3]Texas State University, San Marcos, Texas.
[4]Yurok Tribe.
[5]Hoopa Valley Tribe.

Model selection indicated that the model with density-dependent movement was better supported by the data than density-dependent survival or density-independent movement and survival. Parameter estimates indicated that fry were less likely than parr to move downstream and that fry moved slower. Furthermore, because pools had higher carrying capacity than runs or riffles, juvenile salmon had a lower probability of moving out of pools compared to runs and riffles. This pattern was an emergent property of the model, driven by the combination of the physical habitat structure, the relationship of juvenile salmon abundance to the habitat structure, and the density-dependent movement relationships in S3.

Given that the model was initialized with only the spatiotemporal distribution of spawners, it performed well at capturing the essential outmigration features that are ultimately governed by rates of growth, movement, and mortality. Although the fit to the data was not perfect, the model generally matched observed weekly abundance, migration timing, and size of juvenile outmigrants. The model closely predicted annual abundance in four out of five calibration years, but considerably underpredicted annual abundance estimates of juveniles produced by brood year 2011, the highest abundance year. Higher-than-average survival could have caused this deviation, but underestimation of spawner abundance by monitoring programs may also have contributed. The model matched the weekly abundance and migration timing well, but it tended to underestimate sharp peaks in abundance that were evident in the observed weekly abundance estimates. Lastly, the model underpredicted the mean size of juveniles early in the migration year, but size selectivity of the rotary screw trap towards larger individuals could have contributed to this mismatch.

The Trinity River Restoration Program (TRRP) Science Advisory Board recommended that the TRRP immediately focus on developing core elements of a decision support system (DSS; Buffington and others, 2014). Toward that end, the habitat and S3 models described in this report are both core elements of the DSS. The structure of S3 makes it a particularly useful fish production model for the DSS because population dynamics are sensitive to (1) water temperature, (2) daily flow management, and (3) habitat quality and quantity. Each of these variables are key management parameters under consideration in the TRRP. As such, the S3 model will provide valuable insights into the potentially variable impacts that various management decisions will have in the Trinity River.

Introduction

Background

After more than 150 years of human-caused degradation, an intensive effort is underway to restore the Trinity River watershed and recover its once-abundant salmon runs. Alterations to the river began in the mid-19th century as European settlers arrived with the California Gold Rush. Mining impacts increased into the 20th century, with hydraulic mining of the valley walls along the mainstem corridor and several major tributaries, followed by dredging the river bed in search of placer-gold deposits. Dredge tailings were heaped in massive piles on floodplains adjacent to the river, removing the coarse gravel salmon need for spawning and altering rearing habitat available to juvenile salmonids. With the expansion of European settlement, logging and cattle ranching industries took root in the basin, causing erosion and siltation.

A hundred years after the Gold Rush, the construction of two mainstem dams near Lewiston, California, blocked salmon migrations and altered the hydrology of the Trinity River. Completed in 1964, these projects included a tunnel to divert Trinity River water to the Central Valley for agriculture. Dams and water exports to the Central Valley have regulated and greatly reduced flows of the Trinity River, substantially modifying the historical natural flow regime. Additionally, dams inhibited gravel recruitment and modified natural channel-forming geomorphic processes that give rise to salmon habitat. For nearly two decades, a diverse group representing tribal, federal, state, and local stakeholders have been working to rehabilitate the river and restore salmon populations.

In 2000, the Trinity River Restoration Program (TRRP) was established by the signing of the Trinity River Mainstem Fishery Restoration Record of Decision (U.S. Department of the Interior, 2000), with the purpose of restoring the anadromous salmonid populations to pre-dam levels and supporting dependent tribal, commercial, and recreational fisheries (Trinity River Restoration Program and ESSA, 2009). TRRP's strategy for restoring salmon fisheries is to: (1) restore physical processes to create and maintain freshwater salmonid habitats and (2) meet the flow-dependent needs of salmonids (U.S. Fish and Wildlife Service and Hoopa Valley Tribe, 1999). Actions to implement the restoration strategy include (1) mechanical channel rehabilitation, (2) managing flow releases based on water-year dependent instream allocations and biological and physical management targets, (3) coarse sediment augmentation, and (4) watershed restoration to reduce fine sediment input into the mainstem Trinity River.

The underlying hypothesis of the restoration strategy is that restoring the physical processes (given constraints of the existing infrastructure) and managing flows to meet micro-habitat and thermal needs of anadromous salmonids will provide increased spawning and rearing habitat (Trinity River Restoration Program and ESSA Technologies, Ltd., 2009). In turn, this will lead to increased abundance of high-quality naturally produced juvenile salmonids, ultimately resulting in increased spawners.

The TRRP is implemented under an Adaptive Environmental Assessment and Management (AEAM) framework (U.S. Fish and Wildlife Service and Hoopa Valley Tribe, 1999; U.S. Department of the Interior, 2000). Implementation of the AEAM process is outlined in the TRRP Integrated Assessment Plan (IAP; Trinity River Restoration Program ESSA Technologies, Ltd., 2009). The Integrated Assessment Plan identifies key assessments necessary to provide short-term and long-term feedback on the effectiveness of the TRRP in meeting specific management objectives as well as long-term programmatic goals.

For evaluating management objectives to be implemented by the TRRP, a subcommittee of the TRRP Fish Workgroup was established to initiate the development of a Trinity River fish production model (Trinity River Restoration Program and ESSA Technologies, Ltd., 2009). Recommendations by the TRRP Science Advisory Board (SAB) further motivated the development of a Trinity River fish production model as part of the TRRP decision support system (DSS). The fish production model should enable the TRRP to evaluate:

- Response of fish production to different flow management alternatives, including variable flow levels during specific life history stages;
- Response of fish production to different channel rehabilitation actions;
- Overall restoration strategy of the TRRP using potential habitat estimates to attain fish population goals;
- Temperature response of fish growth and resulting production; and
- Growth/size of fish in response to different flow/temperature alternatives and relate this to potential survival.

Given the required outputs of a fish production model for the TRRP, the Stream Salmonid Simulator (S3) was selected as the modeling framework for the Trinity River DSS. S3 is a population model that simulates daily growth, movement, and mortality of freshwater life stages of riverine salmonids. The model is spatially explicit, representing the river as a linked series of meso-habitat units (MHUs), each with associated discharge, water temperature, and habitat characteristics that are linked to demographic processes to drive population dynamics.

The S3 model is based in concept on SALMOD, a fish production model with a long history in the Klamath Basin (Bartholow and others, 1993; Williamson and others, 1993; Bartholow, 1996; Bartholow and others, 2002). The underlying basis of these fish production models is that daily flows influence the amount of habitat available to different salmonid life stages, and the amount of habitat influences density-dependent process that affect fish production. In developing S3, our goal was to retain the essential ideas behind SALMOD (linking fish habitat to production), but to re-invent the modeling framework to:

1. Develop a more rigorous mathematical basis for spatially explicit population dynamics in a riverine environment;
2. Update movement models to reflect recent advances in modeling juvenile salmon migration;
3. Implement more mechanistic growth models parameterized for anadromous salmonids of interest; and
4. Implement the model in an open-source modeling platform.

We began development of S3 for the Klamath River in 2012, following completion of River Basin Model-10 (RBM10) for the Klamath River (Perry and others, 2011). RBM10 is a spatially explicit water temperature model that provided simulations of daily water temperatures and discharge required as input for the S3 model. Since 2012, our modeling team has developed new growth models for juvenile Chinook Salmon (*Oncorhynchus tshawytscha*)(Perry and others, 2015; Plumb and Moffitt, 2015) and Coho Salmon (*O. kisutch*)(Manhard and others, 2018), new analytical methods for quantifying habitat suitability criteria needed for modeling available fish habitat (Som and others, 2018), and constructed the underlying S3 modeling framework that is implemented in the R statistical programming language (R core team, 2017; Perry and others, 2018a). The application, parameterization, and calibration of S3 to the Klamath River was recently completed (Perry and others, 2018b).

An existing RBM10 water temperature model for the Trinity River (Jones and others, 2016) and the potential to link the Trinity River and Klamath River fish production models made S3 a good choice for the TRRP DSS. The 2017 release of a graphical user interface for RBM10 (https://sites.google.com/site/klamathtrinityinterfacehelp) will provide resource managers a convenient tool to simulate alternative dam operations for the development of alternative water temperature and discharge scenarios for input to the fish production model. In conjunction with S3, these alternative water temperature and discharge scenarios will be helpful in evaluating how Trinity River fish populations respond to alternative management actions. In this report, we describe the construction and calibration of the Trinity River S3 model, using empirical biological data and the historical hydrologic record.

Purpose and Scope

The purpose of this report is to describe the application of the S3 model to the Restoration Reach of the Trinity River (the 64 river kilometers [rkm] downstream of Lewiston Dam). We detail model construction, parameterization, and calibration, and we evaluate how well the production of juvenile Chinook Salmon predicted by S3 compares to observed data. This report is presented as a companion to Perry and others (2018a), which details the general model structure and sub-models that are common across applications of S3 to Chinook Salmon in both the Klamath and Trinity Rivers.

Study Site

The Trinity River in northwestern California is the largest tributary to the Klamath River, with a drainage area of 7,700 square kilometers (km^2). Approximately one-fourth of the Trinity River Basin lies above Lewiston Dam, which is located on the mainstem Trinity River near Lewiston, 181 kilometers (km) upstream of the Trinity-Klamath River confluence. From the confluence, the Klamath River empties into the Pacific Ocean 70 km downstream. Completed in 1963, Lewiston Dam regulates the flow of the Trinity River and stands as an impassable migration barrier to anadromous fish populations. The majority of upstream inflows are first captured and stored by Trinity Dam, which is connected to Lewiston Dam via a reservoir roughly 11 km long.

Native anadromous fish of the Trinity River include Chinook Salmon (*Oncorhynchus tshawytscha*), Coho Salmon (*O. kisutch*), and Steelhead Trout (*O. mykiss*), all of which sustain valuable tribal, commercial, and recreational fisheries. The Trinity Fish Hatchery at the base of Lewiston Dam has supplemented these fish populations to mitigate the loss of upstream fish habitat since 1958, when dam construction began. Coho Salmon belong to the Southern Oregon/Northern California Coast (SONCC) evolutionary significant unit (ESU), listed as threatened since 2005 under the federal Endangered Species Act. Trinity River Chinook Salmon belong to the Chinook Salmon SONCC ESU, and in 1999 a petition for federal Endangered Species Act listing was declined.

The Chinook Salmon population is comprised of two distinct sub-populations: Spring and Fall run. Adult Spring Chinook Salmon return to the Trinity River from April to September, and by July are concentrated in deep cold-water pools near Lewiston Dam. Spring-run fish typically remain in cold-water refugia near the dam for months prior to spawning, which occurs from late September through October. Adult Fall Chinook Salmon return to the Trinity River between August and December, and hold for shorter periods of time prior to spawning. Spawn timing for Fall-run fish typically begins in mid-October, peaks in November, and ends in late December. Spawning activity is concentrated near Lewiston Dam early in the spawning season, and then diffuses throughout the river as the season progresses.

Since 2000, the TRRP has worked to improve and restore fish habitat and to promote fluvial geomorphic processes in the Restoration Reach of river that spans from Lewiston Dam downstream to the confluence with the North Fork Trinity River. This section of river also defines the spatial extent for the current application of S3 for the Trinity River. Fish populations in the Restoration Reach are monitored intensively. Spawner surveys are performed annually to estimate spawner abundance. Juvenile production in the Restoration Reach is monitored using mark-recapture methods and a rotary screw trap fished at Pear Tree Gulch, located about 1 km upstream from the North Fork Trinity River confluence (i.e., near the downstream boundary of the S3 model domain).

Methods

In this section, we describe the details of the S3 model parameterized for Spring and Fall Chinook Salmon of the Trinity River. First we present methods for construction of the habitat template, estimation of habitat capacity, and development of the physical and biological inputs used by S3. Next we briefly describe growth, movement, and survival submodels, detailing values we used for user-defined parameter settings. Third, we define a set of candidate models to test hypotheses about the mechanism by which density dependence affects population dynamics. Last, we describe methods for model calibration and parameter estimation methods, along with the model selection criteria we use to identify which candidate model best fits observed abundance estimates.

Stream Salmonid Simulator Model Inputs

Habitat Template

The spatial domain of the S3 model is defined by a one-dimensional representation of discrete meso-habitat units. MHUs are spatially referenced by their upstream and downstream boundaries measured as the distance in river kilometers from the Klamath River confluence. The length of an MHU is simply the difference between its upstream and downstream boundaries.

To define the MHU boundaries for the Trinity River, field biologists (led by co-author Aaron Martin) who are intimately familiar with the river, delineated MHUs at transitions between three distinct meso-habitat types: riffles, runs, and pools. The Restoration Reach was partitioned into 356 contiguous MHUs classified by meso-habitat type (fig. 1). MHU delineations were drawn perpendicular and normal to the river flow using orthographic satellite imagery and GIS. Disagreements were few and arbitrated via discussion, and ultimately MHU boundaries were decided with full consensus among group members.

To define the quality and quantity of fish habitat within each MHU we utilized output from a 2-D hydraulic model (Bradley, 2016) and micro-habitat models (Som and others, 2018). For this endeavor, we represented each MHU as a polygon (figs. 1 and 2), which allowed us to assign cells of the finer-scale hydraulic model to each MHU. Output from micro-habitat models were then applied to the cells of the 2-D hydraulic model and summarized over each MHU to construct the one-dimensional inputs required by the S3 model.

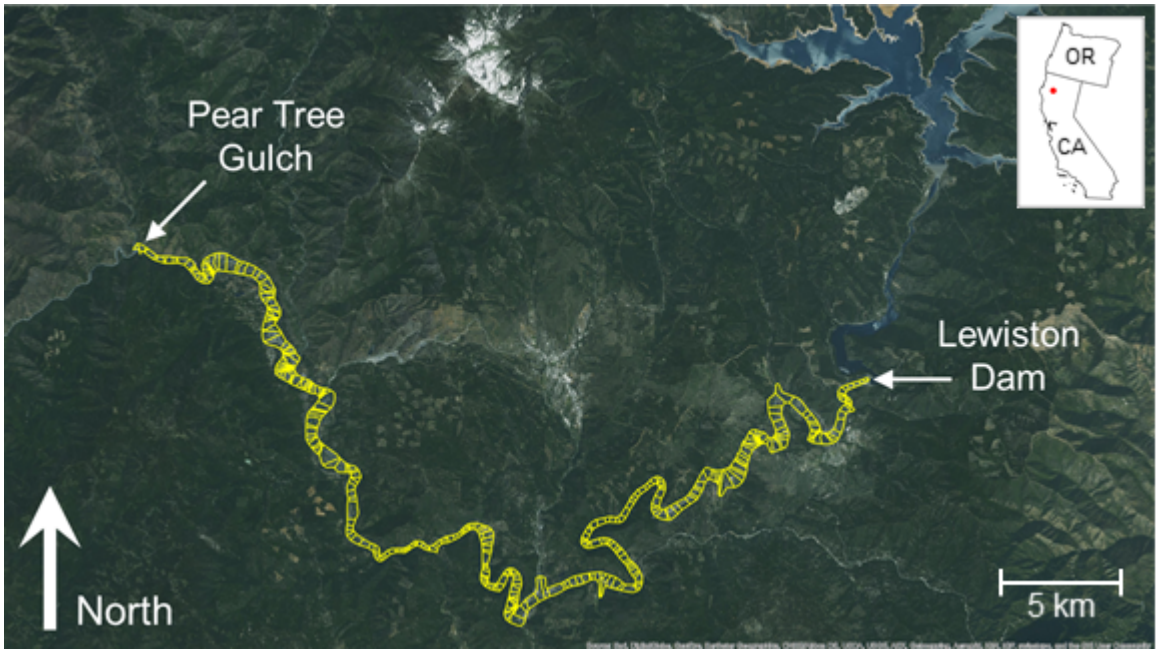

Figure 1. Aerial image of Trinity River, California. The 64-kilometer Trinity River Restoration Reach is highlighted in yellow. The yellow wire mesh shows polygon boundaries of the 356 meso-habitat units that make up the S3 habitat template. The red dot in the inset map shows the location of the study area.

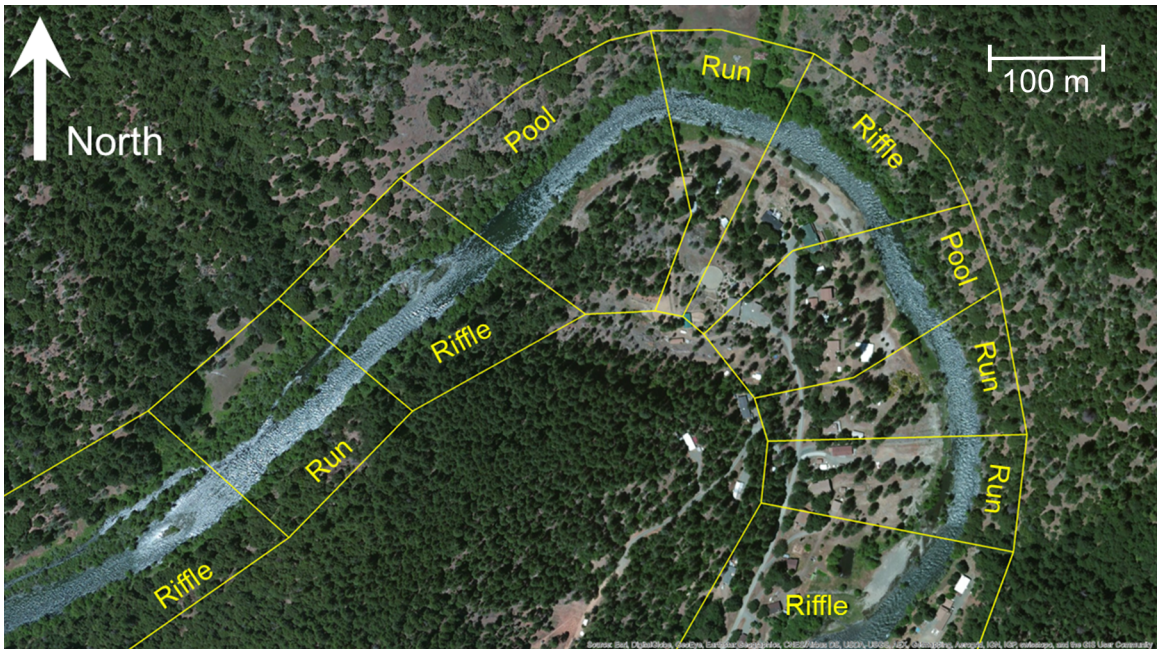

Figure 2. Closeup aerial image showing detail of the Stream Salmonid Simulator habitat template, Trinity River, California. Yellow polygons show meso-habitat units for this section of river and their assigned meso-habitat type.

Physical Inputs

The S3 model requires two physical inputs that drive population dynamics either directly or indirectly: (1) water temperature and (2) streamflow. The S3 model requires these inputs as a timeseries of daily mean water temperature (°C) and daily mean discharge (cubic feet per second [ft^3/s]) for each MHU. We used RBM10 (Jones and others, 2016) to simulate the historical timeseries of temperature and stream flow for the Restoration Reach. Daily mean temperature and daily mean stream flow were output 0.32 rkm downstream of Lewiston Dam and 0.32 rkm downstream of seven mainstem tributaries included in the RBM10 model (table 1). These eight output locations accounted for flow accretions and the associated changes in water temperature. RBM10 output was mapped to each MHU in S3 such that flow and temperature were constant among MHUs between tributaries, but varied among reaches between tributaries (table 1).

Table 1. Tributaries included in the River Basin Model-10 (RBM10) water temperature model that lie within the Trinity River Restoration Reach, RBM10 output locations, and the corresponding Stream Salmonid Simulator meso-habitat units associated with the RBM10 output.
[rkm, river kilometer]

Tributary	Output location (rkm)	Meso-habitat units (range)
Lewiston Dam	178.96	1–36
Rush Creek	172.84	37–71
Grass Valley Creek	166.89	72–144
Indian Creek	152.89	145–152
Weaver Creek	150.63	153–159
Reading Creek	148.86	160–221
Browns Creek	140.82	222–303
Canyon Creek	126.98	304–356

Habitat Capacity

To drive density-dependent population dynamics, S3 requires inputs that define either a daily timeseries of the amount of suitable habitat (m^2) in each MHU or the carrying capacity of each MHU (e.g., an upper limit for the number of redds or number of juveniles that a habitat unit can support). We used micro-habitat models explicitly parameterized for the Trinity River to estimate the carrying capacity of each MHU for juvenile Chinook Salmon life-stages, fry and parr, and we used a multi-scale habitat model to estimate the amount of suitable habitat for the spawning life-stage of Chinook Salmon (Som and others, 2018). These models use a number of key microhabitat variables to develop the flow-capacity or flow-habitat relationships in each MHU: water depth, water velocity, distance to cover, the 84th percentile of substrate composition ("D_{84}"), and the wetted surface area of the MHU. Below, we describe how each of the micro-habitat models were applied to output from Sedimentation and River Hydraulics–Two-Dimension Model (SRH-2D; Lai, 2008, 2010), a two-dimensional hydraulic model that we used to estimate each of the key habitat variables over a range of discharge levels (Lai, 2008; Bradley, 2016).

Estimating Key Habitat Variables with Sedimentation and River Hydraulics–Two-Dimensional Model

We used SRH-2D to simulate habitat variables needed to quantify redd-, fry-, and parr-carrying capacities. The two-dimensional model mesh of SRH-2D was comprised of 1,064,804 computational cells that covered the full extent of the 64-km Restoration Reach (Bradley, 2016). Water depth, water velocity, distance to cover, D^{84} substrate, and wetted surface area were output for each computational cell at 16 levels of stream flow: 300; 450; 550; 700; 800; 950; 1,100; 1,250; 1,500; 2,000; 2,500; 3,500; 4,500; 5,500; 8,500; and 11,000 ft^3/s. A geographic information systems cover layer appended to the SRH-2D computational cells included the "distance to cover" (D_C) variable, which was output for the estimation of fry and parr capacities (Pinnix and others, 2016).

Daily Redd Capacity

The carrying capacity of redds is defined as the maximum number of redds that an MHU can support and was estimated as the amount of suitable redd habitat (square meter [m^2]) divided by mean redd size (4.5 m^2). To estimate the daily amount of suitable redd habitat, we used a logistic regression model developed by Goodman and others (2018) that estimated the probability of redd suitability based on micro-habitat variables collected during redd surveys. The linear predictor for the probability of redd occurrence was:

$$\begin{aligned}\operatorname{logit}\left(p_{\text{redd}}\right) = \quad & 0.860 - 0.227D_{84} - 0.982D_{84}^2 - 0.540D_T + \\ & 0.045D_S - 0.011D_D - 0.428D_S^2 + \\ & 0.240V - 0.285D - 1.177D^2 - 0.023D_S D_D + \\ & 0.013D_D D^2\end{aligned} \tag{1}$$

where

$\operatorname{logit}\left(p_{\text{redd}}\right)$ is the logit transformation for the probability of redd occurrence,

D_{84} is the 84th percentile of gravel/cobble diameter (millimeter [mm]) taken from a representative sample of substrate,

D_T is distance to transition (m),

D_S is distance to shore (m),

D_D is distance to Lewiston Dam (km),

V is water velocity (m/s), and

D is water depth (m).

All variables in this model were standardized to zero mean and unit standard deviation prior to model fitting (see appendix table 1-1).

This redd habitat model was applied to all cells of the SRH-2D model at each level of stream flow. Since DS was not estimated by SRH-2D, we set it to the mean value in the Goodman and others (2018) study. Additionally, values of D84 from SRH-2D that were outside the range of field measurements were truncated to the range of observed field measurements (i.e., between 4 and 250 mm). Given the probability of redd occurrence for each cell and flow level, the amount of suitable redd habitat in each habitat unit was calculated as:

$$A_{\text{redd},h} = \sum_{c=1}^{C_h} a_{c,h} p_{\text{redd},c,h} \tag{2}$$

where

$A_{\text{redd},h}$ is the total amount of suitable redd habitat in unit h, $a_{c,h}$ is the area (m^2) of cell c in habitat unit h,

$p_{\text{redd},c,h}$ is the probability of redd occurrence in cell c of habitat unit h, and

C_h is the total number of computational cells in habitat unit h.

The amount of suitable redd habitat was converted to redd capacity by dividing area $A_{\text{redd},h}$ by the mean size of redds (4.5 m^2).

We then developed a daily timeseries of redd area and capacity by linearly interpolating between the 16 flow-levels at which redd area and capacity were estimated from the SRH-2D model. Redd area and capacity for any daily flows that fell outside the range of flows modeled with SRH-2D were set to values based on the minimum (300 ft^3/s) or maximum (11,000 ft^3/s) SRH-2D flow-levels.

Daily Fry and Parr Capacity

To estimate the carrying capacity of each habitat unit in S3, we used methods developed by Som and others (2018), who developed micro-habitat models of fry density for the Trinity River. The linear predictor of mean fry density from Som and others (2018) was:

$$\begin{aligned}\log(\lambda_{\text{fry}}) = -1.626 - 0.696V + 0.007D - 0.382D_{\text{C}} + 0.159\left(V \times D\right) + \\ 0.089\left(V \times D_{\text{C}}\right) - 0.193\left(D \times D_{\text{C}}\right) + q_p\left(\sigma_{\text{s}}\right) + q_p\left(\sigma_{\text{t}}\right)\end{aligned} \tag{3}$$

where

λ_{fry} is the mean fry density (number of fish per square foot [fish/ft^2]),

V is water velocity (ft/s),

D is water depth (ft), and

D_{C} is distance (ft) to nearest cover.

The final term in the model quantifies observed variation in mean density over space and time, where

$\sigma_{\text{s}} = 0.406$ is the standard deviation associated with spatial variation in mean density,

$\sigma_{\text{t}} = 0.507$ is the standard deviation associated with temporal variation in mean density, and

q_p is a quantile associated with the standard normal distribution for a given cumulative probability p (for example, $q_{p=0.5} = 0$).

For parr, we fit micro-habitat models using the same methods that Som and others (2018) developed for fry. The linear predictor of parr density was:

$$\log(\lambda_{\text{parr}}) = -3.177 - 0.713V + 0.342D - 0.630D_{\text{C}} + 0.125(V \times D) - 0.072(V \times D_{\text{C}}) - 0.154(D \times D_{\text{C}}) + q_p(\sigma_{\text{s}}) + q_p(\sigma_{\text{t}}) \quad (4)$$

where

$\sigma_{\text{s}} = 0.734$, and

$\sigma_{\text{t}} = 0.153$.

In S3, we implement fry and parr capacity as an upper bound to the number of fish a given habitat can support (number of fish per square mile). In the model of Som and others (2018), variation in micro-habitat fish density is modeled as arising from a Poisson distribution with a mean density of λ, so we estimated capacity by first calculating the 95th percentile of mean abundance by setting p = 0.95 and $q_{p=0.95} = 1.96$ in eqn. 3 and 4, and then using the 95th percentile of the Poisson distribution evaluated at the mean abundance with $q_{p=0.95} = 1.96$ as an estimate of carrying capacity for each cell in the SRH-2D model.

Daily MHU capacities of fry and parr were constructed using SRH-2D output in the same manner as for redd capacity. First, capacity was estimated for each of the SRH-2D cells at each of the 16 flow-levels. Given the capacity for each cell and flow level, the carrying capacity for fry and parr in each habitat unit was calculated as:

$$K_{\lambda,h} = \sum_{c=1}^{C_h} a_{c,h}\lambda_{c,h} \quad (5)$$

where

$K_{\lambda,h}$ is the carrying capacity of fry or parr in habitat unit h, $a_{c,h}$ is the area (m^2) of cell c in habitat unit h,

$\lambda_{c,h}$ is the estimated maximum fry or parr density in cell c of habitat unit h, and

C_h is the total number of computational cells in habitat unit h.

SRH-2D cells predicted to exceed the estimated maximum fish density of Som and others (2018), due to physical characteristics outside the range of observed values from the sampling of Som and others (2018), were set to the estimated maximum to prevent extrapolating outside the range of the micro-habitat model. Using the field-measured model covariates, the maximum density estimate was 27.4 and 8.8 fish/ft^2 (294.9 and 94.7 fish per square meter), for fry and parr, respectively.

We then developed daily time-series of fry and parr capacity by linearly interpolating between the 16 flow-levels at which fry and parr capacities were estimated from the SRH-2D model. Fry and parr capacities for any daily flows that fell outside the range of flows modeled with SRH-2D were set to values based on the minimum (300 ft^3/s) or maximum (11,000 ft^3/s) SRH-2D flow-levels.

Biological Inputs

The S3 model relies on the three forms of biological inputs to simulate population dynamics. These biological inputs include (1) female spawners, (2) juvenile hatchery fish releases, and (3) juveniles entering from tributaries. Methods detailing spawners and hatchery releases are detailed below. For the Trinity River implementation of the S3 model covering the Restoration Reach, we did

not include juveniles entering from tributaries for two reasons. First, consistent annual estimates of spawner and outmigrant abundances do not exist for most tributaries in the Restoration Reach. Second, model development collaborators from within the TRRP deemed any tributary production too small to be of consequence to the dynamics of fish emerging from mainstem redds or released at the hatchery.

Female Spawners

To develop inputs for the number of female spawners, spawner survey data (Chamberlain and others, 2012) was summarized as a weekly time-series of redd counts by survey reach. Of the 14 spawner survey reaches between Lewiston Dam and the Klamath River confluence, 7 reaches fall within the Restoration Reach (table 2). We modeled two distinct spawning sub-populations in S3, early and late spawners, which generally track the timing of spawning of Spring and Fall Chinook Salmon. Because Spring and Fall Chinook Salmon redds cannot be visually differentiated, the State of California's Department of Fish and Wildlife (CDFW) estimates a spawning cut-off date (for example, fig. 3) that determines when redds switch from being classified as Spring Chinook Salmon to Fall Chinook Salmon. CDFW generates this cut-off date based on coded-wire tag recoveries collected at the hatchery (Borok and others, 2014). To assign spawners to sub-populations in S3, we adopted the cut-off dates provided by CDFW. Although we label the early and late-spawning populations as "Spring" and "Fall" Chinook in this report, we recognize that a simple cut-off date does not capture overlap in the temporal spawning distribution of Spring and Fall Chinook Salmon. Furthermore, the cutoff date based on hatchery returns may not be representative of the timing of in-river spawning. Therefore, although we label the modeled populations as "Spring" and "Fall," the reader should recognize that the S3 model is tracking the progeny of these early (Spring) and late (Fall) spawners based on the cutoff date provided by CDFW and shown in figure 3.

To construct model inputs, we mapped the reach-level redd survey data to each MHU and converted the weekly redd counts to daily redd counts by dividing weekly counts by seven. Within each survey reach, daily redds were then distributed to MHUs proportional to the distribution of daily redd capacity in each survey reach.

Table 2. Location of redd survey reaches and the associated Stream Salmonid Simulator (S3) habitat units, Trinity River, California.

[rkm, river kilometer]

Survey reach	Upstream boundary (rkm)	Downstream boundary (rkm)	Meso-habitat units
1	180.57	177.36	1–19
2	177.36	170.25	20–51
3	170.25	159.48	52–107
4	159.48	149.00	108–160
5	149.00	134.61	161–257
6	134.61	125.99	258–309
7	125.99	116.56	310–356

Trinity River Hatchery Releases

We included hatchery releases of age 0 (fingerling) juvenile Chinook Spring and Fall Chinook Salmon as separate sub-populations in S3. Data on hatchery releases of Chinook Salmon were obtained from the Regional Mark Information System database (http://www.rmpc.org/). Juvenile Chinook Salmon from the Trinity River Hatchery were released in batch releases that were predominantly volitional in nature. Volitional releases were initiated by opening a gate on a hatchery pen so fish could freely enter the Trinity River. On average, 12 days lapsed (range: 8–17 days) before the last fish exited the pen. As a result, each release was associated with a start and end date. We approximated the daily number of fish released by partitioning the batch size evenly across the days of the volitional release. Typically, more than one batch was released at a time. For input to S3, the total number of hatchery fish entering the river each day was the sum of the daily approximated number of fish released from all concurrent batches. The Trinity River hatchery also releases cohorts of several other salmonid species throughout the year, but intereactions of these salmonids with Chinook Salmon is not currently modeled in S3.

In addition to daily hatchery release numbers, S3 required the mean weight of hatchery fish entering the river. Prior to release, each batch was sampled to estimate the mean weight of individual fish. To calculate the mean weight of fish entering the river in S3, we used the mean weight of fish in concurrent batch releases, weighted by the batch-specific daily release numbers. Daily release numbers and weighted-mean fish weights were computed separately for Spring and Fall Chinook Salmon. Simulated hatchery inputs entered the river just below the dam (MHU = 1), and the two sub-populations were tracked separately in S3. The mean weight of fish was converted to fork-length (FL) to classify the life-stage of hatchery inputs as fry, parr, or smolt, upon river entry.

Stream Salmonid Simulator Submodels and User-Defined Parameter Settings

When simulating fish populations with S3, some population dynamics are dictated via user defined options and parameter inputs. Juvenile fish populations in the S3 model are affected by three dynamic processes: (1) survival, (2) growth, and (3) movement. Below, we describe how the submodels were parameterized for the Trinity River and specify values of user-defined parameters. For details on the mathematical structure of individual submodels, we encourage readers to consult Perry and others (2018a).

Spawning, Egg Development, and Egg Survival Submodels

The number of eggs that survive to emerge as fry is affected by several S3 parameters and submodels. We set the fecundity of female spawners to 3,000 eggs per redd to approximate the mean number of eggs observed for Chinook Salmon returning to the Trinity River Hatchery from 2000 to 2015 (Spring Chinook Salmon, mean = 2,970 eggs; Fall Chinook Salmon, mean = 3,046 eggs). The mean time from spawning to fry emergence is modeled as a function of daily water temperature and accumulation of degree days (see Perry and others, 2018a). Variation in emergence timing is assumed to follow a normal distribution about the mean emergence date and is controlled by the standard deviation in degree days required to hatch, which we set to 26.6 degree days. Bias in simulated emergence timing can arise when intra-gravel temperatures are warmer or cooler than the surface water temperature used to model egg development. In a recent study, David (2017) found that intra-gravel temperatures in the

Trinity River tend to be warmer than the surface water during fall and winter months (i.e., during the incubation period) and to be more than 3 °C warmer at some locations. To accommodate the temperature differential, S3 enables the user to apply an intra-gravel temperature offset. We set the intra-gravel temperature offset to +1 °C.

During the incubation period, S3 includes three mechanisms that affect egg-to-fry survival: (1) baseline "natural" mortality, (2) temperature-related mortality, and (3) redd superimposition (Perry and others, 2018a). The natural mortality rate was set at 0.25 percent per day, which equates to a baseline survival rate of about 92.8 percent per month. Thermal tolerance parameters were set so that water temperatures less than or equal to 17 °C had no effect on egg survival, but temperatures greater than 17 °C imposed a daily mortality rate of 25 percent (Geist and others, 2006).

Redd superimposition is the process whereby a later arriving spawner builds a redd on top of an existing redd and dislodges or entombs the eggs laid by the earlier spawner. Superimposotion is modeled in S3 as a function of habitat capacity and spawner abundance. The probability of redd superimposition is defined by redd density (redd abundance/redd capacity), which is calculated and applied daily for each MHU. The amount of redd mortality attributed to superimposition on day t is simply the number of redds to be recruited that day multiplied by the existing pre-recruitment redd density. However, given the propensity of Chinook Salmon to guard their redds until death, the S3 model allows the user to set a "guarding period" parameter. We set the guarding period to 10 days, assuming that semelparous Chinook Salmon live to guard their nests for 10 days after spawning. Redds are not vulnerable to superimposition during the guarding period.

Although redd scour owing to freshets is known to influence survival of eggs, we have not yet implemented mortality owing to scour in the Trinity River S3 model. We have investigated several scour functions for the Trinity River during the model development phase, but have not included those models because there is little evidence for significant redd scour in brood years we used for calibration. We anticipate that a future version of the S3 model will include an egg-scour function.

Juvenile Growth

S3 provides two options for temperature-driven growth models: the Ratkowsky Model and the Wisconsin Bioenergetics Model (Perry and others, 2018a). Mean fish size for each source population and life stage in each habitat unit was incremented daily as a function of water temperature using the Wisconsin Bioenergetics Model with a revised consumption function (Plumb and Moffitt, 2015). For application to the Trinity River, we fixed the proportion of maximum consumption parameter to 0.66 and set all other parameter values to those listed in Perry and others (2018a). Under this parameterization, the Wisconsin and Ratkowsky growth models exhibit similar growth rates over a range of water temperatures (Perry and others, 2018a). The growth model governs life-stage transitions by moving fish to the next life stage when their mean size exceeds user-defined size thresholds for each life stage. For our simulations, the juvenile life-stage classifications were fry: fork length (FL) $\leq$ 50 mm; parr: 50 < FL $\leq$ 90 mm; and smolt: FL > 90 mm. For natural-origin fish, we set the weight of emergent fry to 0.3 grams, which back-calculates to a fork-length of 30 mm (see appendix figs. 1-1–1-9). The mean size of fry, parr, and smolt were recomputed daily within each MHU to account for daily growth, growth-based life-stage transitions, recruitment of emergent fry, and movement among habitat units. We assumed that the growth model applied uniformly to all juvenile life-stages, natural- and hatchery-origin fish, and Spring and Fall Chinook Salmon sub-populations.

Juvenile Movement

S3 has two submodels for simulating fish movement: (1) the "mover-stayer" model, and (2) the "advection-diffusion" model (Perry and others, 2018a). In both models, movement from one MHU to another is simulated in the downstream direction only. In our simulations, we used the mover-stayer model for rearing fry and parr, and the advection-diffusion model for actively migrating smolts. The mover-stayer model can be implemented with density-independent or density-dependent movement, which is a user-specified option. With density-independent movement, abundance and capacity have no effect on movement probability. Density-independent movement is the only option available with the advection-diffusion model.

Two parameters drive movement in the mover-stayer model: (1) the probability of remaining in the currently occupied MHU (P^{stay}) from time t to t+1 (resulting in "stayers"), and (2) the mean distance moved downstream (i.e., resulting in "movers"; kilometers per day). For the density-dependent form of the model, P^{stay} is expressed as a Beverton-Holt function such that P^{stay} declines as the ratio of abundance to capacity increases. That is, the probability of moving (1-P^{stay}) increases as abundance approaches capacity. We estimated theP^{stay} parameter for density-dependent and density independent forms of the mover-stayer model. The mean distance moved was calculated deterministically as a function of fork-length, using the same size-based movement rate as we used for the smolt life stage, as described in Perry and others (2018a).

We modeled smolt movement using a density-independent advection-diffusion process because this model was developed for actively migrating smolts, not smaller rearing fish that are less likely to move downstream (Zabel and Anderson, 1997; Zabel, 2002). The advection-diffusion model assumes that the spatial distribution of a population at a given point in space after t time units is described by a normal distribution with a mean location and standard deviation. We allow the movement rate of smolts to depend on size, with the rate of movement increasing with fish size. The parameters of this model were based on size relationships developed by Zabel (2002) and Plumb (2012) for juvenile Snake River Fall Chinook Salmon (Perry and others, 2018a).

Juvenile Survival

Daily survival probability, like movement probability, can be specified either as density-independent or density-dependent. In the density-dependent form, survival probability is expressed as a Beverton-Holt function that decreases as the ratio of abundance to capacity increases (Perry and others, 2018a). In this form, we estimate S^0, the expected survival as abundance approaches zero. In the density-independent form, daily survival probability is estimated as a constant value that does not depend on abundance or habitat capacity. Under both forms of the survival model, parameters may be allowed to differ among life-stages and source-populations. Parameters of the survival model were estimated via calibration, which is described below. We compare alternative models that use either the density-independent or density-dependent form of the survival model. Additionally, we allow the parameters to vary among life stages and source populations.

Calibration and Model Selection

The goal of calibration is to estimate survival and movement parameters of the S3 model by fitting the model to estimates of weekly abundance of juveniles passing a rotary screw trap located near Pear Tree Gulch at the downstream terminus of the Restoration Reach (henceforth, "Pear Tree trap"). We fit the model to 5 years of weekly abundance estimates (brood years 2006 and 2008–11). These years were selected based on the completeness and robustness of the juvenile abundance estimates. To fit the model to abundance estimates, we used a likelihood function where deviations between simulated and estimated weekly abundances followed a normal distribution:

$$\hat{N}_{w,y} = \tilde{N}_{w,y}\left(\boldsymbol{\theta}\right) + \varepsilon_{w,y} \tag{6}$$

where

$\hat{N}_{w,y}$ is the number of juveniles estimated to have passed the trap site in week w of year y,

$\tilde{N}_{w,y}\left(\boldsymbol{\theta}\right)$ is the simulated number of juvenile salmon passing the trap site in week w of year y for a given vector of parameters $\boldsymbol{\theta}$, and

$\varepsilon_{w,y}$ is a normally distributed error term with mean zero and standard deviation σ.

We use the "tilde" notation here to indicate quantities simulated by S3, and the "hat" notation to indicate that true abundances are not known, but are estimated with uncertainty. We account for the uncertainty in estimated abundances using a weighted likelihood for the errors (Deriso and others, 2007):

$$-\ln L\left(\boldsymbol{\theta} \mid \hat{N}_{w,y}\right) \propto \sum_{y}\sum_{w}\left[\ln\left(w_{w,y}\sigma\right) + \frac{\left[\hat{N}_{w,y} - \left(\tilde{N}_{w,y}\left(\boldsymbol{\theta}\right)\right)\right]^2}{2w_{w,y}^2\sigma^2}\right] \tag{7}$$

where

$-\ln L\left(\boldsymbol{\theta} \mid \hat{N}_{w,y}\right)$ is the negative log-likelihood of the parameters given the observed data, and

$w_{w,y}$ are weights that are proportional to the uncertainty in each $\hat{N}_{w,y}$.

For weights, we applied the coefficient of variation, $w_{w,y} = \mathrm{CV}(\hat{N}_{w,y})$, since the standard errors of $\hat{N}_{w,y}$ increase with $\hat{N}_{w,y}$.

The residual standard deviation, σ, can be estimated analytically using:

$$\hat{\sigma} = \sqrt{\frac{1}{n}\sum_{y}\sum_{w}\frac{\left[\hat{N}_{w,y} - \left(\tilde{N}_{w,y}\left(\boldsymbol{\theta}\right)\right)\right]^2}{w_{w,y}^2}} \tag{8}$$

where

n is the total number of abundance estimates across weeks and years.

We used standard optimization routines in R (R core team, 2017) to maximize the likelihood with respect to the parameters.

Although the S3 model simulates daily abundance by life stage and source population (Spring Chinook Salmon, Fall Chinook Salmon, natural-origin, and hatchery-origin), weekly abundance estimates ($\hat{N}_{w,y}$) were aggregated over all life stages and over Spring and Fall Chinook Salmon, but were separated for natural- and hatchery-origin fish. Consequently, for fitting the model to observed data, $\tilde{N}_{w,y}(\boldsymbol{\theta})$ represents the total simulated abundance passing the Pear Tree trap, summed over life stages, over Fall and Spring Chinook Salmon, and over days within weeks, but kept separate for natural- and hatchery-origin fish.

To estimate unique parameters for natural- and hatchery-origin fish, we constructed a separate likelihood for each rearing origin, and the total negative log-likelihood was the sum of the log-likelihoods for natural- and hatchery-origin fish. Additionally, based on weekly fork-length distributions, we noted that the weekly abundance estimates early in the migration season included a small fraction of large fish that were likely age-1 fish that had over-wintered. Since the S3 model simulated age-0 fish, we adjusted the weekly abundance estimates downward by estimating the weekly fraction of large fish likely to be age 1.

Candidate Models

To determine which formulation of the survival and movement parameters best explain the dynamics of the juvenile Chinook Salmon outmigration, we fit a set of four candidate models to the weekly abundances at the Pear Tree trap. The four candidate models represented different combinations of density-independent or density-dependent survival or movement: (1) density-independent survival and movement, (2) density-independent survival and density-dependent movement, (3) density-dependent survival and density-independent movement, and (4) density-dependent survival and movement (table 3). By fitting different combinations of density-dependent movement and survival models to the same data set, we could compare the fit of the different candidate models to the data and evaluate which combination best explained the weekly abundances of fish passing the trap.

We assumed *a priori* that movement and survival parameters differed by life-stage and among hatchery and natural-origin populations, yielding six estimated parameters for each model (table 3). Each model estimated three movement parameters and three survival parameters. For movement, we estimated a unique P^{stay} for natural-origin fry and parr. We also estimated a unique P^{stay} parameter that was common for both hatchery-origin fry and parr because that vast majority of hatchery releases were of parr size, and there was not enough data on hatchery fry to estimate unique parameters for each life stage. Movement parameters of both natural- and hatchery-origin smolts were fixed according to the advection-diffusion model described in Perry and others (2018a). For survival, unique parameters were estimated for natural-origin fry. However, we estimated common survival parameters for parr and smolt life-stages because there was not enough information in the trapping data to estimate unique survival parameters for these life stages. A third common survival parameter was estimated for hatchery-origin fry, parr, and smolt because the calibration routine had difficulty estimating unique survival parameters of hatchery-origin fish by life stage.

Table 3. Candidate S3 models that were fit to weekly estimated abundances at the Pear Tree trap on the Trinity River, California.

[**Model**: *S*, survival; *M*, movement; I, density-independent; D, the density-dependent model forms; *g*, indicating a group-effect for different source-populations (natural or hatchery origin); *a*, life-stage effect for different juvenile life-stages (fry, parr, and smolt); *, a parameter relationship between the group- and age-effects that allows life-stage specific parameters to differ among hatchery- and natural-origin fish populations]

Model No.	Model	Number of parameters
1	$S_I(g*a)$, $M_I(g*a)$	6
2	$S_I(g*a)$, $M_D(g*a)$	6
3	$S_D(g*a)$, $M_I(g*a)$	6
4	$S_D(g*a)$, $M_D(g*a)$	6

We compared the relative rank of each candidate model using Akaike information criterion (AIC), where the lowest AIC value indicates the model with the most support given its fit to the data and the number of parameters (see Burnham and Anderson, 2002). This selection criterion is calculated as $\mathrm{AIC} = -2\log(L(\hat{\theta} \mid x)) + 2K$, where K is the number of estimated parameters, and $\log(L(\hat{\theta} \mid x))$ is the maximized log-likelihood for the given set of estimated parameters ($\hat{\theta}$) and the given data set (x). In this model selection framework, the best model has the lowest AIC score, and models within 2 AIC points are deemed competitive alternatives.

Results

Stream Salmonid Simulator Model Inputs

Biological Inputs

Female Spawners

Female spawner abundance in the Restoration Reach ranged from 2,662 to 4,564 spawners among the 5 calibration years (figs. 3–4). Based on the cut-off date defining Spring and Fall Chinook Salmon, Spring Chinook spawners outnumbered Fall Chinook spawners every year (fig. 3). Spring Chinook spawn timing ranged from late September through October, while Fall Chinook spawn timing extended from early November through late December (fig. 3). Based on redd surveys in seven reaches of the Restoration Reach, spawner abundance was concentrated in the first 5 kilometers downstream of Lewiston Dam and widely dispersed further downstream (fig. 4).

Trinity River Hatchery Releases

Trinity River Hatchery released two to three times as many juvenile Fall Chinook Salmon as Spring Chinook Salmon, depending on the year (table 4). Annual releases of juvenile Spring Chinook Salmon ranged from 662,000 to 948,000 whereas releases of Fall Chinook Salmon ranged from 1.8 to 2 million. Based on the mean size of release groups, there was considerable variation among years in the life stage at which Spring Chinook Salmon were released. In 2 of the years, only smolts were released; in 2 other years only parr were released; and in 1 year about 60 percent more parr than smolts were released. In contrast, for Fall Chinook Salmon, hatchery releases were comprised of parr exclusively in all calibration years.

Physical Inputs

Water temperature and river discharge exhibited similar temporal and spatial patterns across calibration years. Water temperature generally increased in a downstream direction during summer months and approached a maximum daily temperature of 20 degrees at Pear Tree Gulch (fig. 5). There was little spatial variation in water temperature from late fall through spring. At Lewiston Dam, river flows were driven solely by dam operations where the spring freshet occurred at the beginning of May each year, as dictated by the TRRP Record of Decision (fig. 6). However, winter and spring freshets from tributary inputs were evident in Trinity River flows at Pear Tree Gulch (the downstream end of the Restoration Reach), driving variation in the timing and magnitude of freshet flows among calibration years.

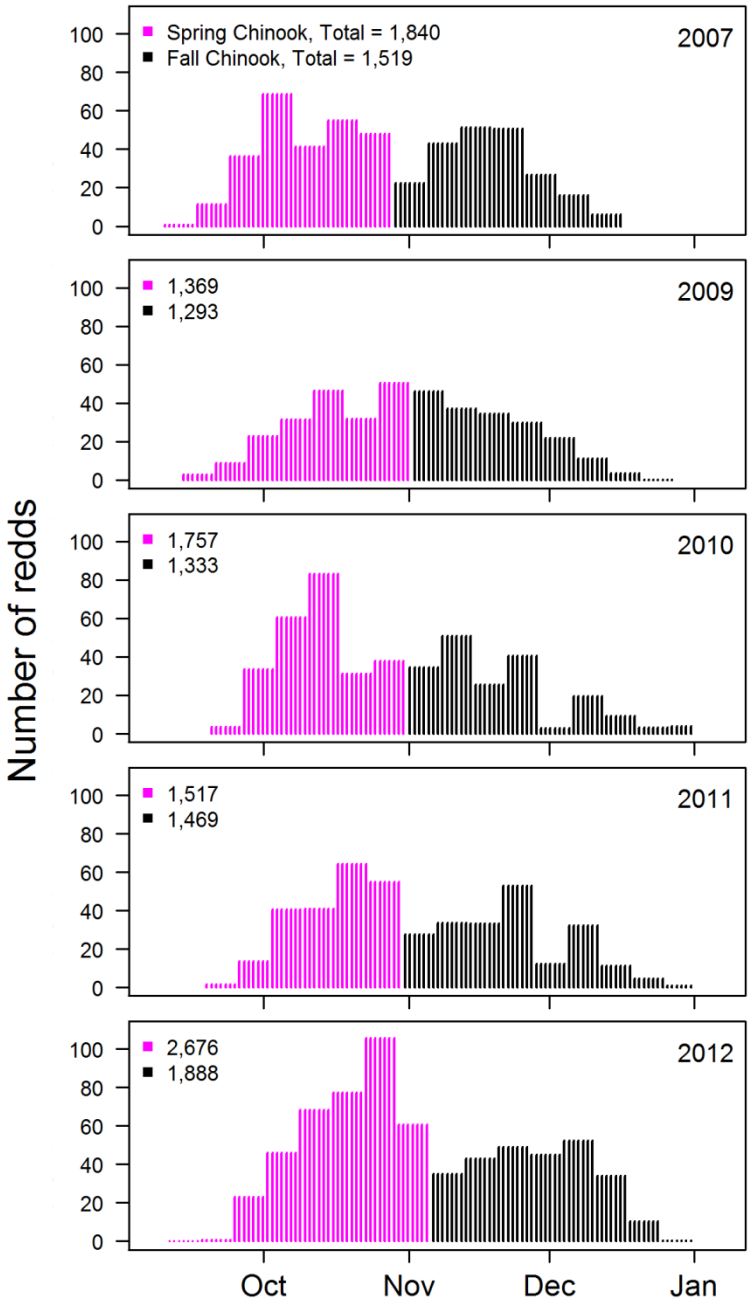

Figure 3. Bar plots showing the temporal distribution of redd counts in the Trinity River Restoration Reach for Spring and Fall Chinook Salmon during the 5 calibration years. Bars represent the weekly observed redd counts distributed uniformly across each day of the week for all seven survey reaches combined.

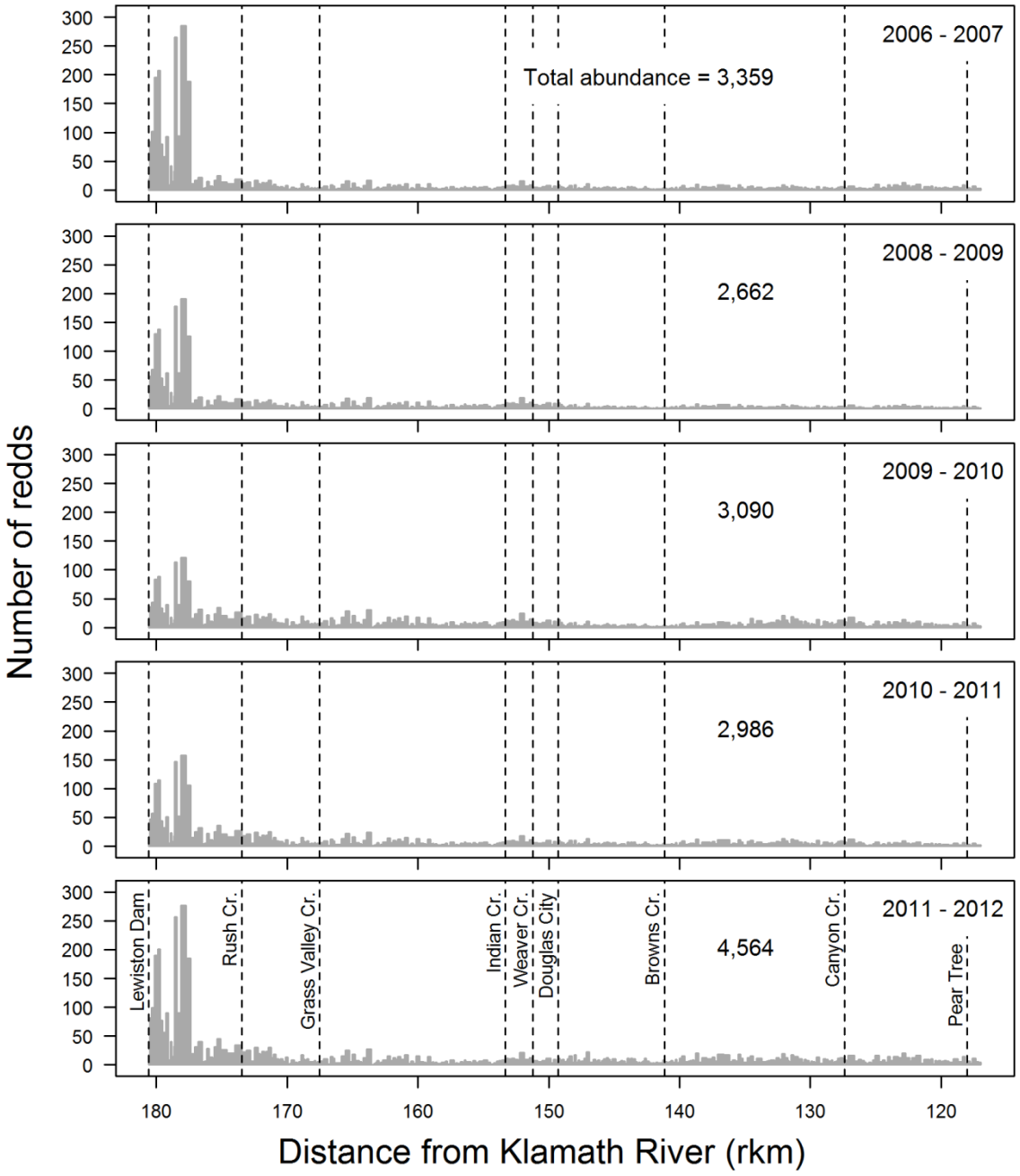

Figure 4. Bar plots showing the spatial distribution of Chinook Salmon redd abundance used as inputs for S3 for 5 spawning seasons, Trinity River, California. Bar-widths are scaled relative to meso-habitat unit length.

Table 4. Annual abundance of Spring and Fall Chinook Salmon by life stage (fry, parr, and smolt) released from the Trinity River Hatchery.

Brood year	Release dates	Fry	Parr	Smolts	Total
Hatchery-origin Spring Chinook Salmon					
2006	June 1–8, 2007	0	947,501	0	947,501
2008	June 1–15, 2009	0	0	940,937	940,937
2009	June 1–8, 2010	0	0	662,155	662,155
2010	June 1–17, 2011	0	728,305	0	728,305
2011	June 1–15, 2012	0	469,349	287,361	756,710
Hatchery-origin Fall Chinook Salmon					
2006	June 1–8, 2007	0	2,021,056	0	2,021,056
2008	June 1–15, 2009	0	2,108,579	0	2,018,579
2009	June 1–8, 2010	0	1,975,162	0	1,975,162
2010	June 1–17, 2011	0	1,936,150	0	1,936,150
2011	June 1–15, 2012	0	1,836,291	0	1,836,291

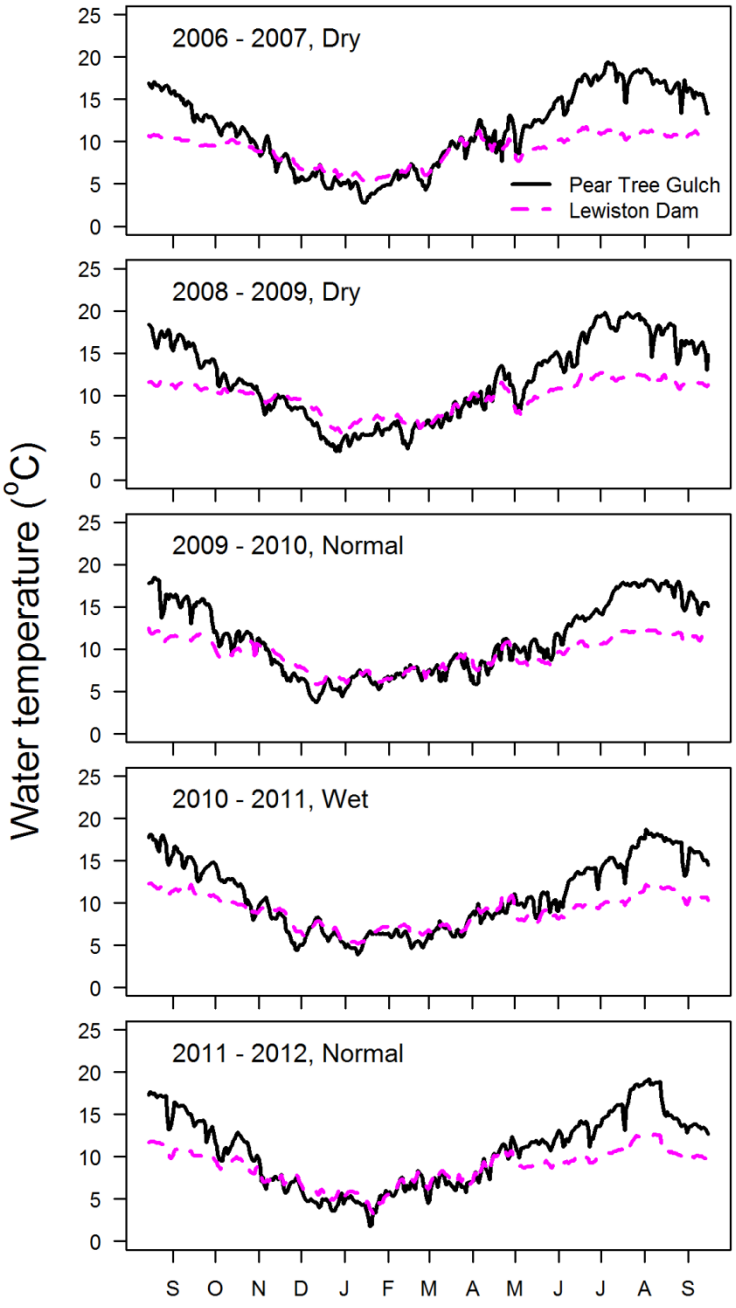

Figure 5. Daily mean water temperature simulated by River Basin Model-10 (RBM10) for each of the 5 brood years used to calibrate the Stream Salmonid Simulator (S3) model, Trinity River Restoration Reach, California. Two of the eight RBM10 output locations within the Restoration Reach are shown: Lewiston Dam (river kilometer 180) and Pear Tree Gulch (river kilometer 127), bracketing the upstream and downstream boundaries of the S3 model domain. Tick marks on the x-axis indicate the first day of each month.

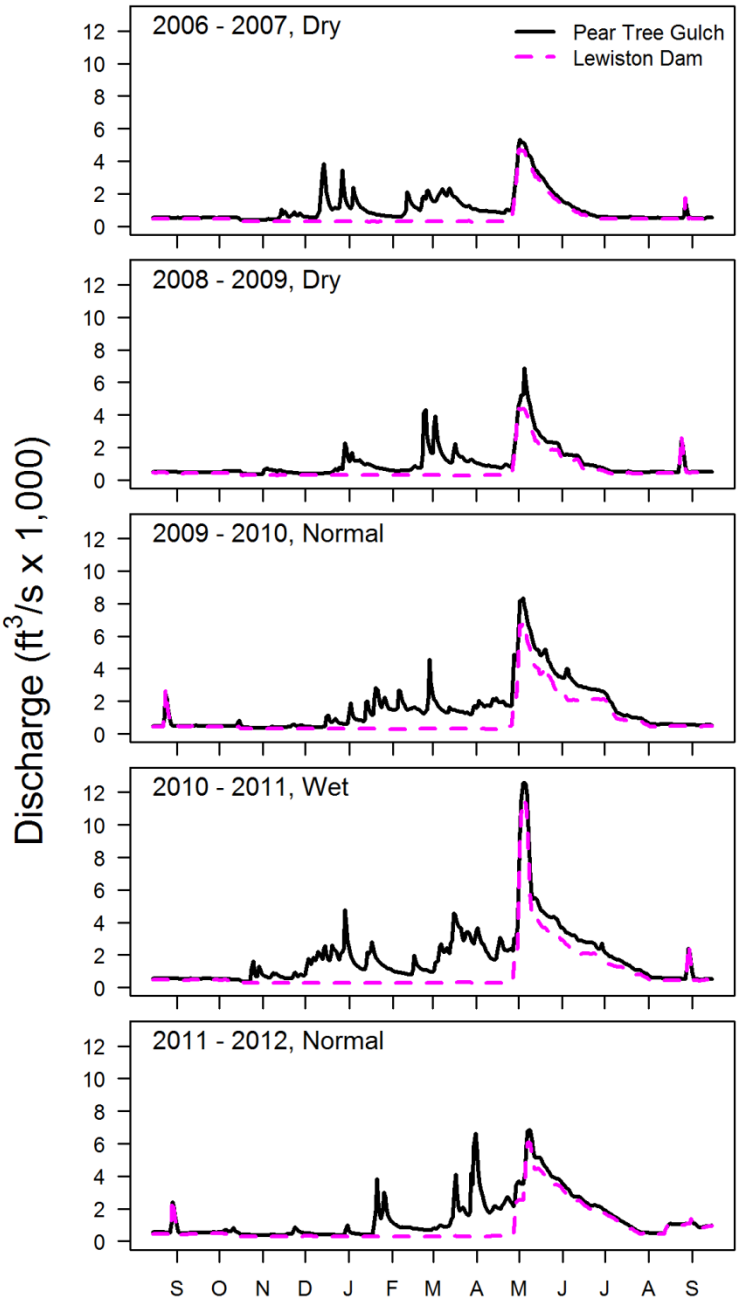

Figure 6. Daily mean discharge simulated by the River Basin Model-10 (RBM10) model for each of the 5 brood years used to calibrate the Stream Salmonid Simulator (S3) model, Trinity River, California. Two of the 8 RBM10 output locations within the Restoration Reach are shown: Lewiston Dam (river kilometer 180) and Pear Tree Gulch (river kilometer 127), bracketing the upstream and downstream boundaries of the S3 model domain. Tick marks on the x-axis indicate the first day of each month.

Habitat Capacity

The time-series of total redd capacity revealed that capacity was inversely related to discharge such that redd capacity is highest at relatively low flows (figs. 6–7). For example, redd capacity peaked at flows less than 1,000 ft^3/s, and then rapidly declined at higher rates of discharge (figs. 6–7). In the years we used for model calibration, discharge was typically low and redd capacity high in the fall and early winter when spawning occurs (figs. 6–7). The bulk of Chinook Salmon spawning habitat was located in MHU's classified as riffles, followed by runs, and then pools (fig. 8).

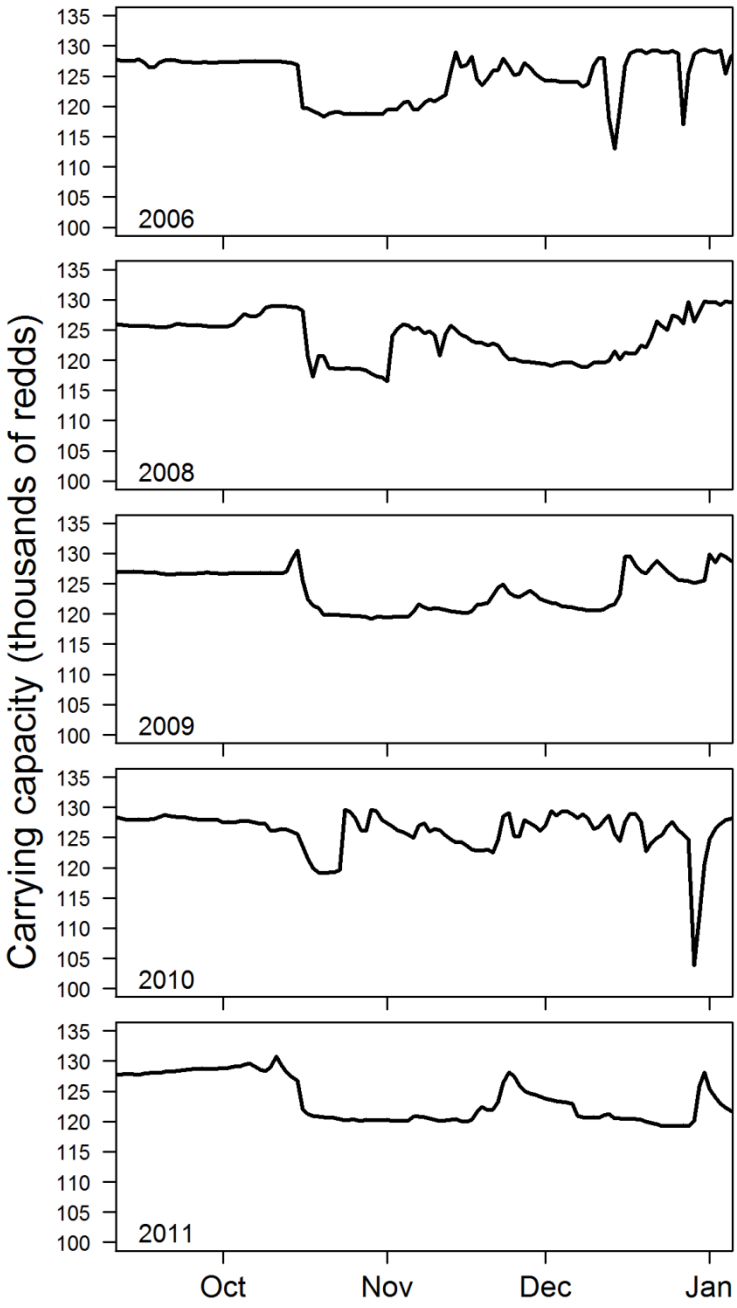

Figure 7. Time-series of total redd capacity within the Trinity River Restoration Reach for the 5 years used in Stream Salmonid Simulator model calibration. Redd capacity was summed for all 356 meso-habitat units. Tick marks on the x-axis indicate the first day of each month.

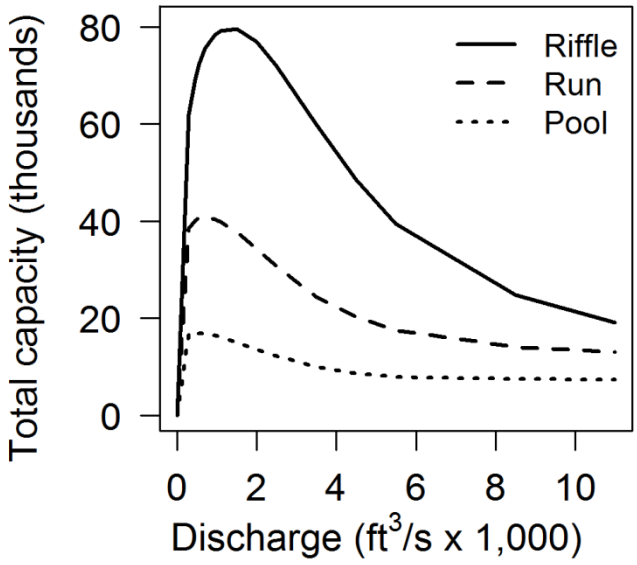

Figure 8. Total redd capacity as a function of stream flow, Trinity River Restoration Reach, California. Capacities were summed by meso-habitat type (riffle, run, and pool) to show differences in the relative capacity among the three habitat types within the Restoration Reach.

Carrying capacity for fry was consistently higher than for parr, but the temporal pattern was similar. Time-series of total fry and parr capacity mimicked the pattern of the hydrograph, with capacities increasing as a function of river discharge (figs. 6, 9). At base flow, fry capacity was about double the capacity of parr.

Summaries of fry and parr capacity by meso-habitat type reveal differences in the quality of habitat available for juvenile fish rearing in riffles, runs, and pools. When capacity is expressed in terms of fish density by scaling relative to the area of each habitat unit (number of fish/m^2), pools exhibited the highest capacity for both fry and parr, followed by runs and riffles (fig. 10). When summing total capacity across all habitat units, riffles and runs had a higher total capacity than pools when flows exceeded 4,000–5,000 ft^3/s. However, there is relatively little difference in total capacity among habitat types when flow is less than 4,000 ft^3/s (fig. 11).

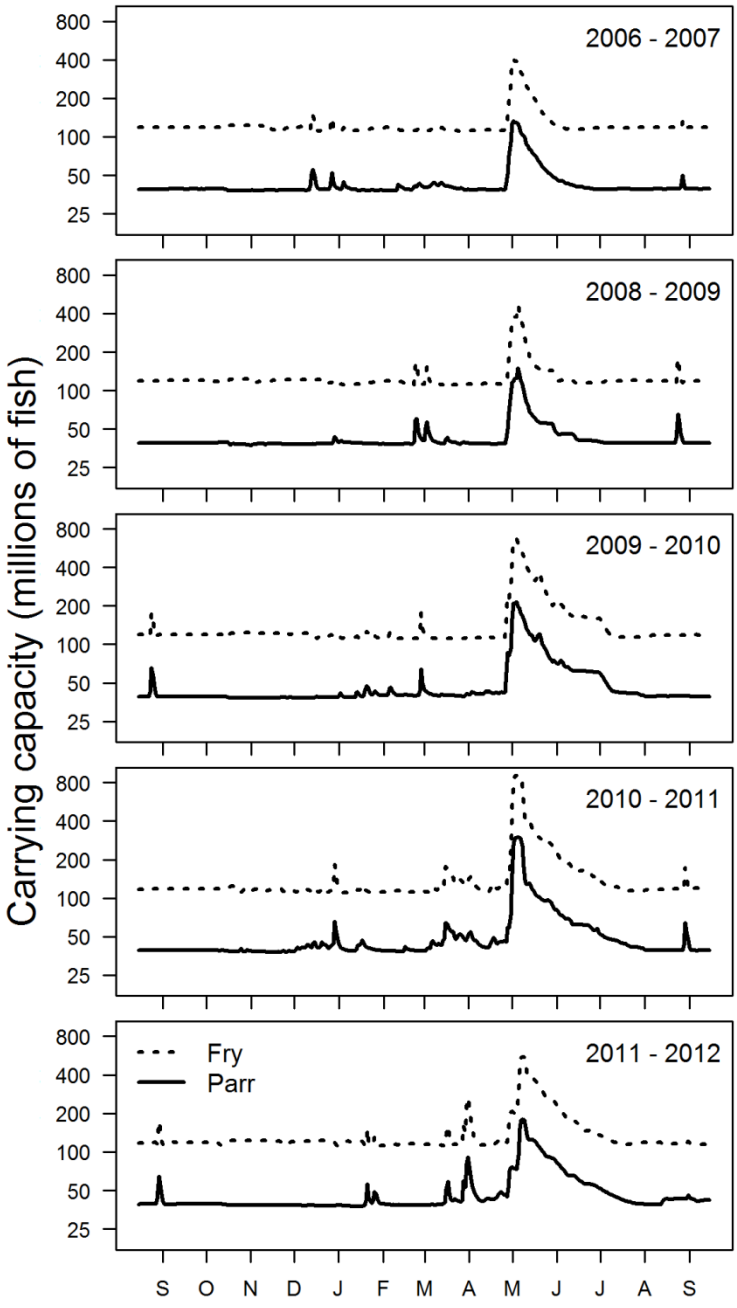

Figure 9. Timeseries of the total capacity of Chinook Salmon fry and parr in the Trinity River Restoration Reach (log-scale), simulated for each of the five hydrographs used to calibrate the Stream Salmonid Simulator model. Tick marks along the x-axis align with the first day of each month.

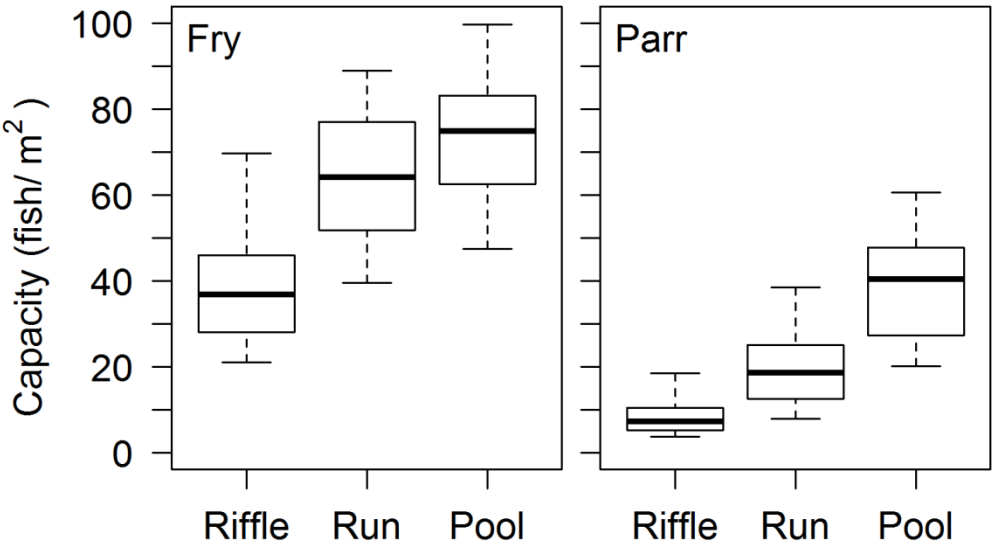

Figure 10. Boxplots of Chinook Salmon fry and parr carrying capacity within riffles, runs and pools of the Trinity River Restoration Reach, California. Heavy horizontal lines show the median. Box hinges show the 25th–75th percentile range. Whiskers bound the 5th–95th percentile range of habitat capacity. Boxplot statistics were computed from the daily capacity estimates of the 356 meso-habitat units based on the five annual hydrographs used for calibration.

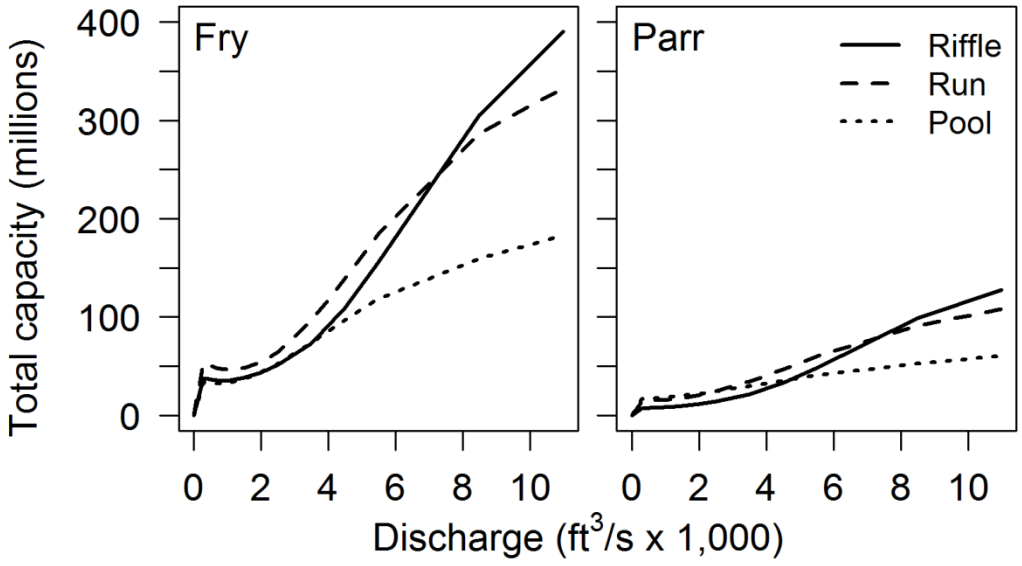

Figure 11. Total fry and parr carrying capacity as a function of stream flow, Trinity River Restoration Reach, California. Capacities were summed by meso-habitat type (riffle, run, and pool) to show relative differences in total capacity as a function of flow.

Egg-to-Fry Survival and Fry Emergence

Total egg-to-fry survival was driven largely by the daily baseline rate of mortality, except near Lewiston Dam where the effect of redd superimposition was substantial. Based on the length of the incubation period, the baseline egg-to-fry survival rate was about 73 percent throughout most of the Restoration Reach for both Spring and Fall Chinook Salmon populations (fig. 12). Egg mortality due to redd superimposition was directly proportional to redd density. In the upper 3 km near the dam where redd densities were highest (fig. 4), egg-to-fry survival was much lower. There was also a notable difference in survival rates between the two sub-populations in the near dam vicinity (fig. 12). Near the dam, Fall Chinook Salmon egg-to-fry survival was about 1–6 percent lower than the 73 percent baseline rate, depending on the year. Because of earlier spawn timing (fig. 3), Spring Chinook Salmon redds near the dam were especially vulnerable to superimposition, experiencing a 2–13 percent lower egg-to-fry survival rate than the later spawning Fall Chinook Salmon (fig. 12). The negative effect of redd superimposition was most pronounced in the 2011–12 season of greatest redd abundance (fig. 12). Because temperatures never exceeded 17°C during the incubation period, temperature-induced egg mortality was never triggered.

Temporal and spatial patterns of fry emergence were dependent upon spawn timing, water temperature, and the spatial distribution of redds. Despite the lack of overlap in simulated spawn timing, variation in the accumulation of degree days required led to overlap in emergence time of Spring (early spawning) and Fall (late spawning) Chinook Salmon (fig. 13). Emergence timing was more protracted for the earlier spawning Spring Chinook Salmon, due to colder water temperatures experienced during incubation (figs. 3, 5, and 13). For the 5 simulated brood years of the two sub-populations, large interannual variation in emergence times occurred. Year-to-year variation in the onset of fry emergence differed by as much as 1 month (fig. 13) and was consistent with differences in spawn timing among years (fig. 3). Spring Chinook Salmon fry began to emerge from the gravel in early December or January, depending on year. Fall Chinook Salmon began to emerge in early February or March. Because the spatial distribution of emergent fry matched the pattern of redd abundance, a relatively large portion of the naturally spawned fish population was produced in the upper 3 km of the Restoration Reach (fig. 14).

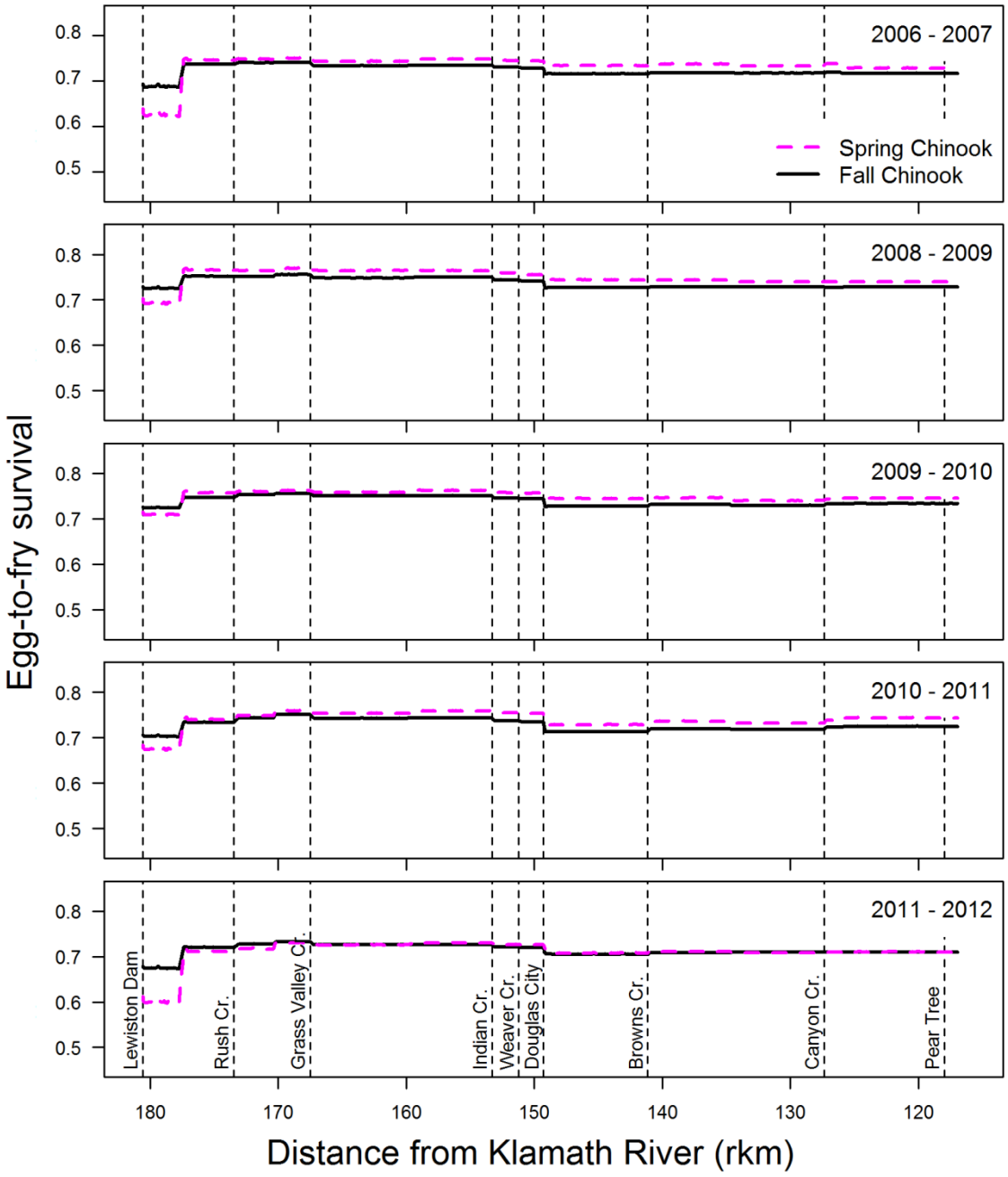

Figure 12. Simulated spatial distribution of egg-to-fry survival of Spring and Fall Chinook Salmon across the 356 meso-habitat units of the Trinity River Restoration Reach, California, for each of the 5 calibration years.

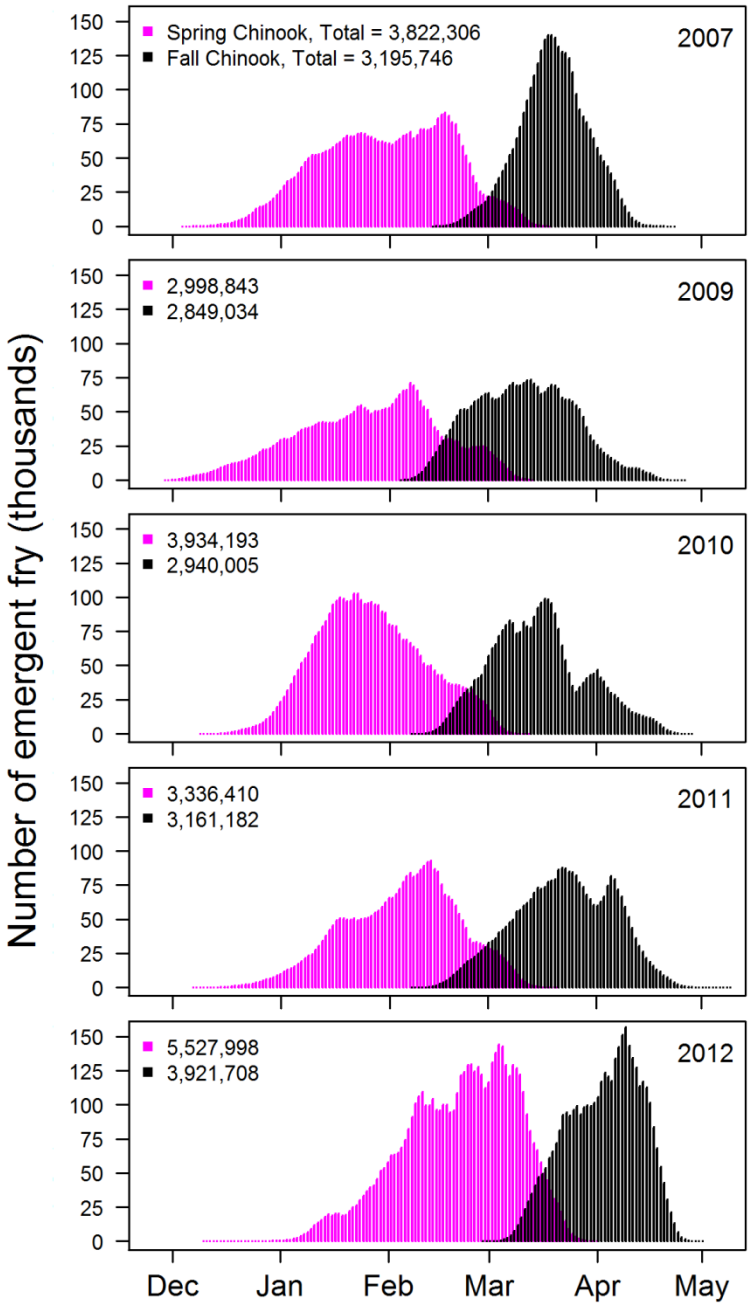

Figure 13. Bar plots showing the simulated timing and abundance of Spring and Fall Chinook Salmon fry emergence, Trinity River Restoration Reach, California, for each of the 5 calibration years.

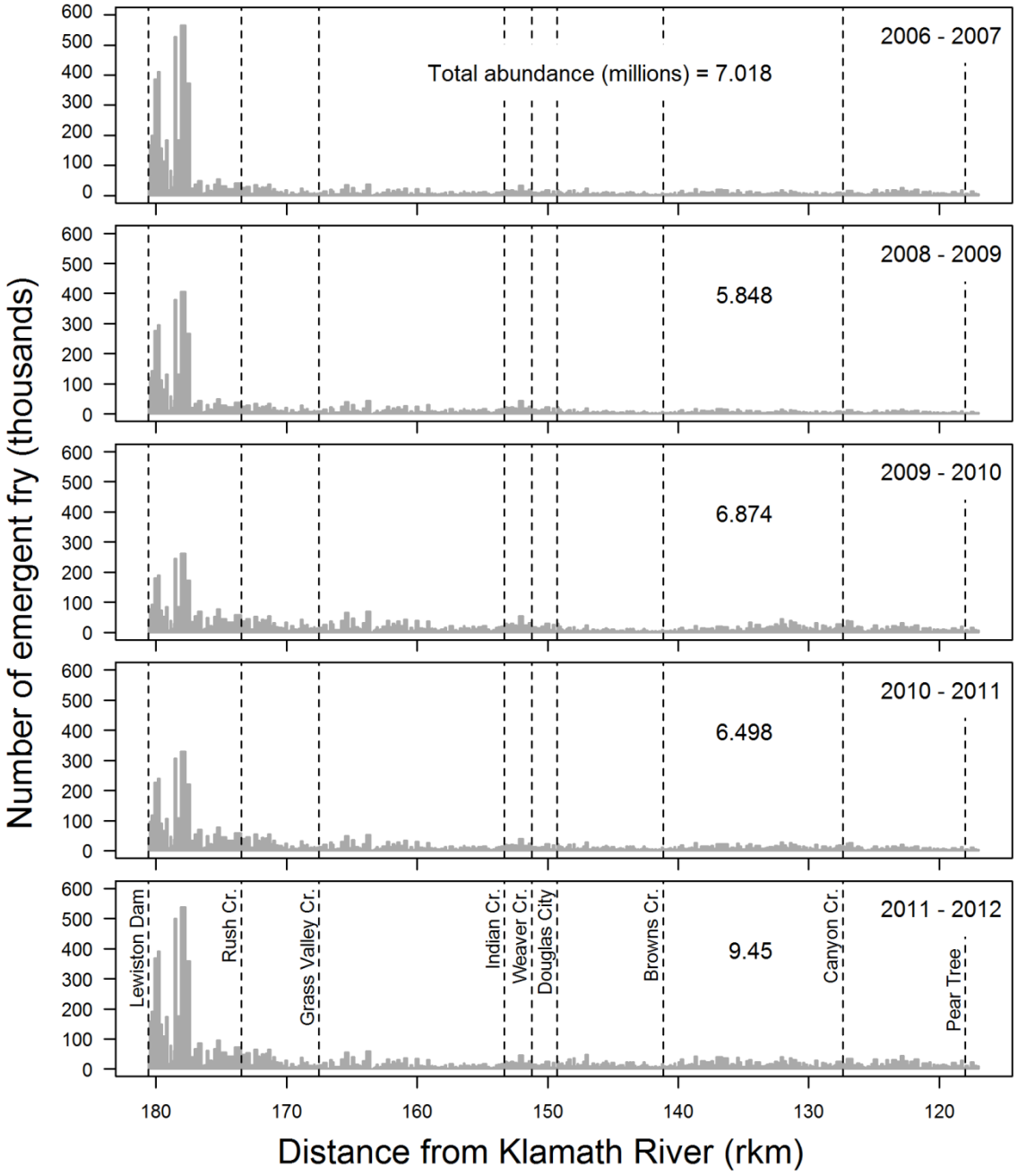

Figure 14. Bar plots of the spatial distribution of simulated fry emergence, Trinity River Restoration Reach, California, for each of the 5 calibration years. Bar-widths are scaled in proportion to the length of each of the 356 habitat units.

Calibration, Model Selection, and Parameter Estimates

Of the four candidate models, two competitive models had much lower AIC values than the two other models (table 5). We found that the best-fit, lowest-AIC model consisted of density-dependent movement and density-independent survival (AIC = 5590.106). We present the model rankings in terms of ΔAIC (AIC minus best model AIC; table 5). The two models that included density-dependent mechanisms for survival performed substantially worse than the models with density-independent survival mechanisms (ΔAIC > 30). The second best model (ΔAIC = 0.538) included density-independent survival and movement mechanisms and matched the estimated weekly abundances at Pear Tree nearly as well as the best model (ΔAIC < 2). Thus, model selection results provided strong evidence that the survival rate was independent of fish density, and some evidence that the movement rate is linked to fish density. Hereafter, we present results based on the best-fit candidate model.

Table 5. Model selection results for the set of candidate models ranked by Akaike Information Criterian (AIC) minus best model AIC, where smaller values indicate better support for a given model fitted to the weekly trap-abundance data.

[**Model**: *S*, survival; *M*, movement; $_I$, density-independent; $_D$, the density-dependent model forms; *g*, indicating a group-effect for different source-populations (natural or hatchery origin); *a*, life-stage effect for different juvenile life-stages (fry, parr, and smolt); *, a parameter relationship between the group- and age-effects that allows life-stage specific parameters to differ among hatchery- and natural-origin fish populations]

Model No.	Model	Number of parameters	Δ AIC
2	$S_I(g*a)$, $M_D(g*a)$	6	0
1	$S_I(g*a)$, $M_I(g*a)$	6	0.538
4	$S_D(g*a)$, $M_D(g*a)$	6	30.518
3	$S_D(g*a)$, $M_I(g*a)$	6	30.524

Parameter estimates of the best-fit model suggested differences in movement and survival parameters between life stages and between natural- and hatchery-origin fish (table 6). Parameter estimates of the movement model indicated that hatchery fish were less likely than natural-origin fry and more likely than natural-origin parr to remain in a given MHU (table 6). For natural-origin juveniles, fry and parr had a 48 and 1 percent holding probability intercept, respectively (table 6). Since holding probability was expressed as a density-dependent function, movement probability (1-P_{stay}) increased with density. Furthermore, because capacity differed among habitat types, juvenile salmon had the highest probability of moving out of riffles and the lowest probability of moving out of pools, but the effect of density was negligible for natural-origin parr (figs. 10 and 15), as their probability of moving remained high regardless of density. Estimates of daily survival probability for natural-origin fish were consistently higher than for hatchery fish, regardless of life-stage. For naturally spawned fish, the daily survival rate was about 99 percent for fry and 90 percent for parr and smolt. In comparison, the estimated daily survival rate was 85 percent for hatchery fry, parr, and smolt (table 6).

Table 6. Parameter estimates of movement and survival for the best-fit model (Model 2).

[**Model parameter**: Parameters of the best model included density-dependent movement processes and density-independent survival; $P_{\text{stay},0}$, indicates that the parameter estimate refers to the intercept of the Beverton-Holt model, defined as P_{stay} at zero abundance.]

Model parameter	Source population	Life-stage	Estimate	Standard error
Holding probability ($P_{\text{stay},0}$)	Natural	Fry	0.476	0.0028
	Natural	Parr	0.010	0.0282
	Hatchery	Fry, parr	0.279	0.0295
Daily survival probability (S)	Natural	Fry	0.987	0.0011
	Natural	Parr, smolt	0.889	0.0168
	Hatchery	Fry, parr, smolt	0.848	0.0148

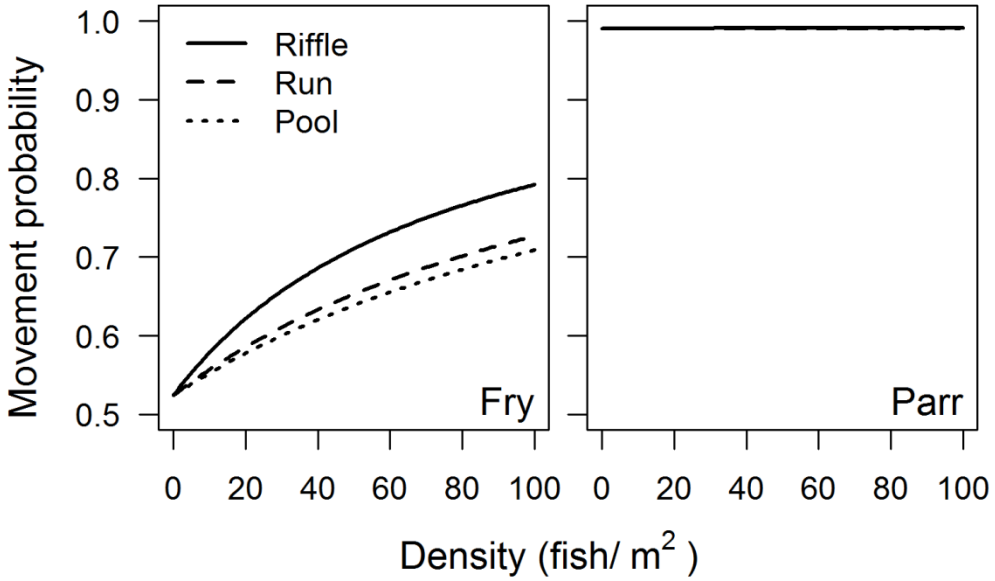

Figure 15. Natural-origin Chinook Salmon fry and parr movement probability shown as a function of fish density and meso-habitat type based on the density-dependent movement parameters estimated for the best Stream Salmonid Simulator life-cycle model, Trinity River, California. Plot lines are based on the median capacity (fish per square meter [fish/ m^2]) of each habitat type (riffle, run, and pool) computed for the five calibration hydrographs.

Goodness of Fit

Although our best candidate model ranked substantially better than the alternative models with a density-dependent survival mechanism, AIC rank is not by itself a measure of how well the best fit model fits the observed data. In the following section we compare different metrics to gauge model performance, with a focus on the simulated versus estimated juvenile Chinook Salmon abundance, migration timing, and size of populations passing Pear Tree Gulch.

Simulated and Estimated Abundance

Comparison of simulated and estimated total annual abundances showed that the S3 model performed well in most years, but underestimated total abundance considerably in 2012 (fig. 16). In 2012, a year of exceptionally high abundance, the simulated abundance of natural-origin fish was 2,105,146 less than the observed abundance estimate. For all other years, simulated annual abundance agreed closely with observed annual abundance estimates for both hatchery- and natural-origin fish, although a slight tendency to underpredict was exhibited (fig. 16).

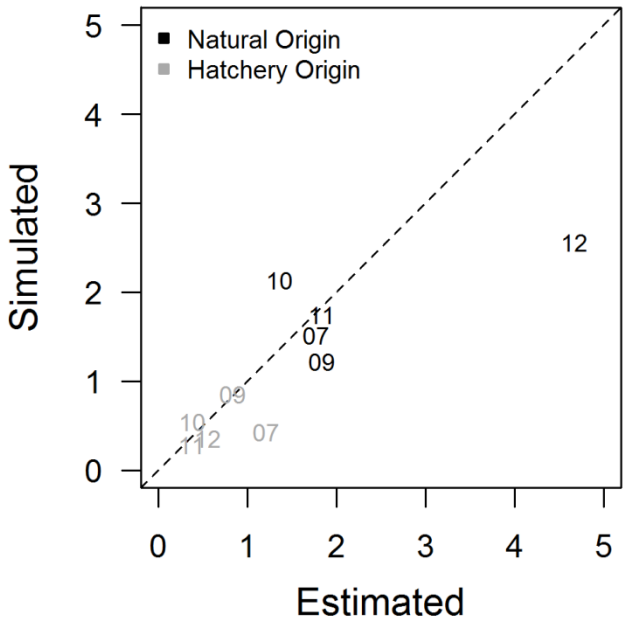

Figure 16. Simulated and estimated total annual abundance (millions) of natural- and hatchery-origin juvenile Chinook Salmon passing Pear Tree Gulch (rkm 117.9) during the 5 calibration years, Trinity River, California.

Comparison of simulated and estimated weekly Pear Tree Gulch abundances indicated generally good model performance for both natural- and hatchery-origin populations. On the scale of original units, there was little evidence of heteroscedasticity in residuals, and, aside from 2012, simulated versus estimated weekly abundances appeared evenly distributed about the line of unity (fig. 17, left-panel). For 5 or more weeks during the 2012 outmigration, simulated weekly abundances of natural-origin fish were much less than the observed abundance estimates. There was a tendency for S3 to substantially underpredict the peak observed estimates of weekly abundance, and several of those weeks occurred in 2012. Expressing simulated versus estimated abundances on a log-scale revealed a tendency for simulated abundance to underpredict observed abundance estimates when abundance was low (<100,000 fish; fig. 17, right-panel). Simulated weekly abundances were reasonably well synchronized with observed weekly abundance (figs. 18–19), although there was a lag in rising limb of abundance in most years and simulated weekly abundance followed a smoother time trend relative to sharp peaks in the observed weekly abundance estimates.

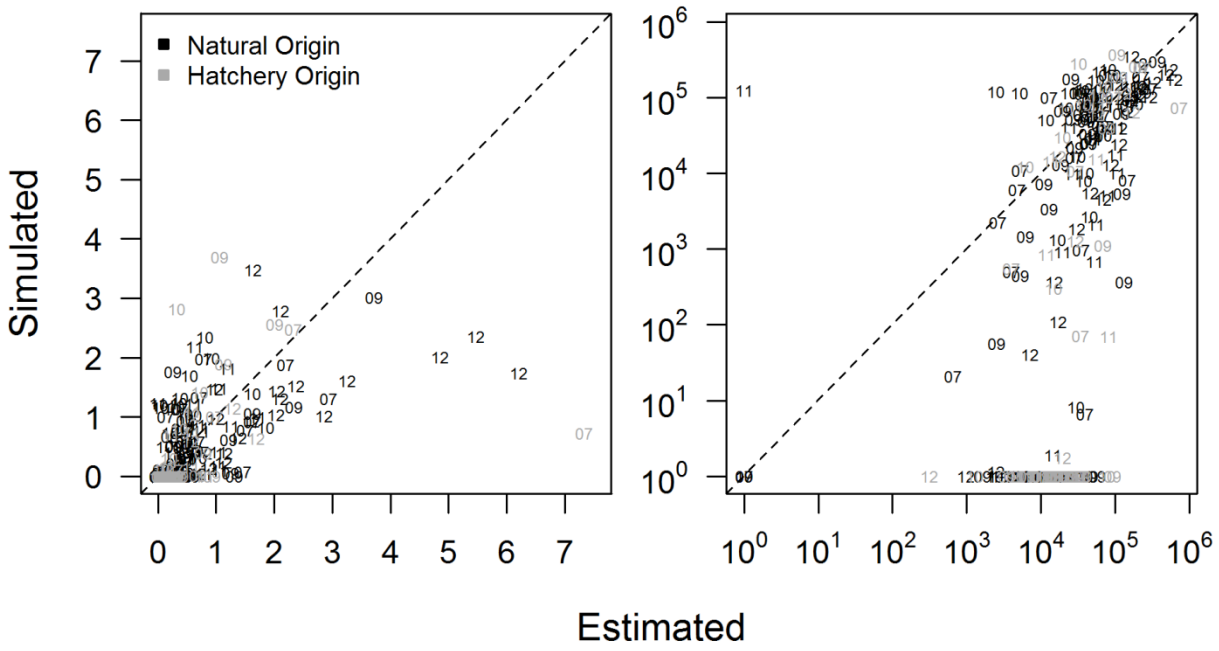

Figure 17. Stream Salmonid Simulator simulated and estimated weekly abundance of natural- and hatchery-origin juvenile Chinook Salmon source populations at Pear Tree Gulch (rkm 117.9), during the 5 calibration years. Weekly abundances are for fry, parr, and smolt age-classes combined (left panel, hundred thousands; right panel, log-scale), Trinity River, California.

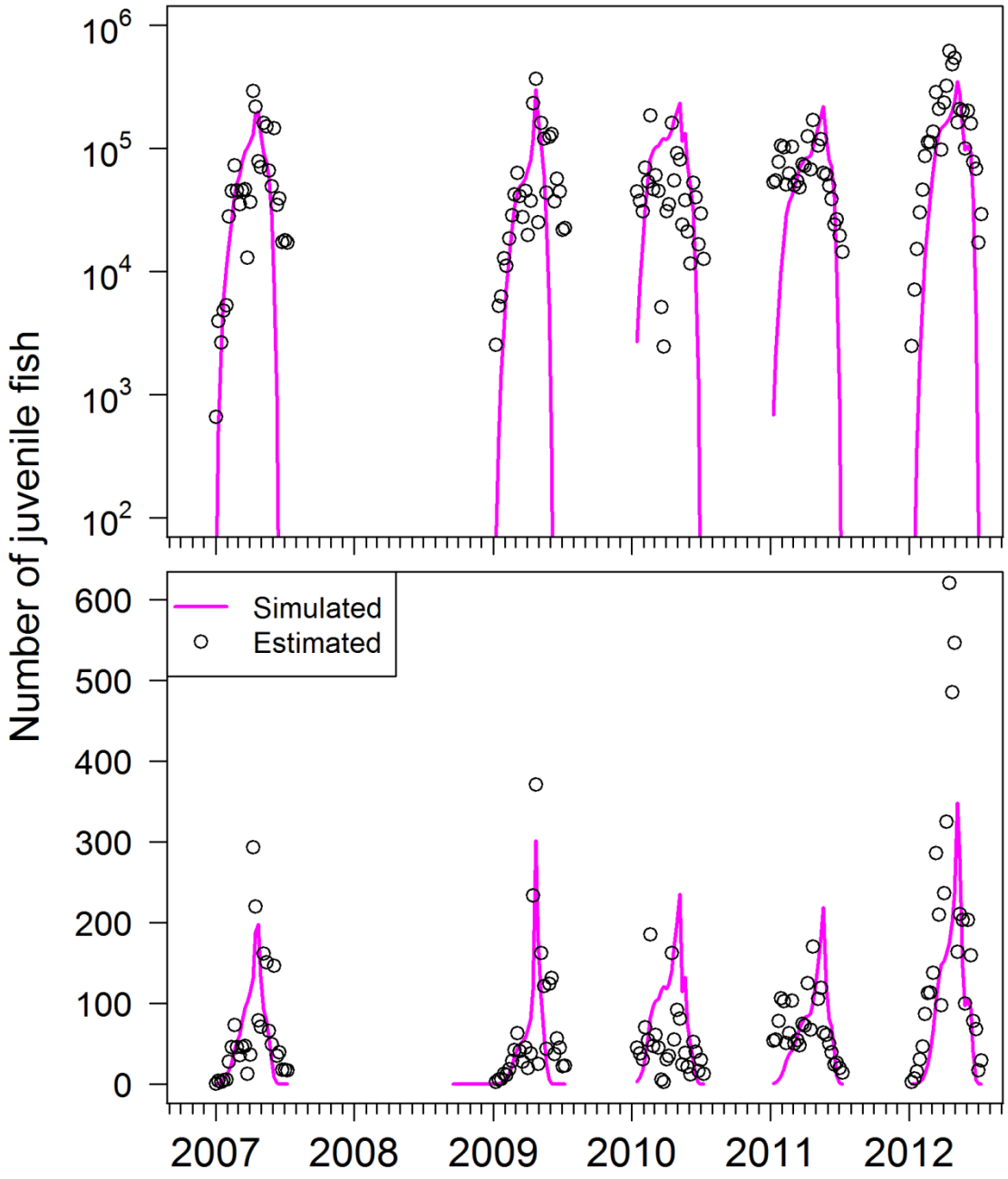

Figure 18. Timeseries plots of simulated weekly abundance of natural-origin juvenile Chinook Salmon passing Pear Tree Gulch (rkm 117.9) and screw-trap mark-recapture based point estimates for each of the 5 calibration years. Major tick marks are aligned at January 1 of each year along the x-axis, minor tick marks align with the first day of each month. Abundance is plotted on a log-scale (upper panel) and in original units (thousands; lower panel).

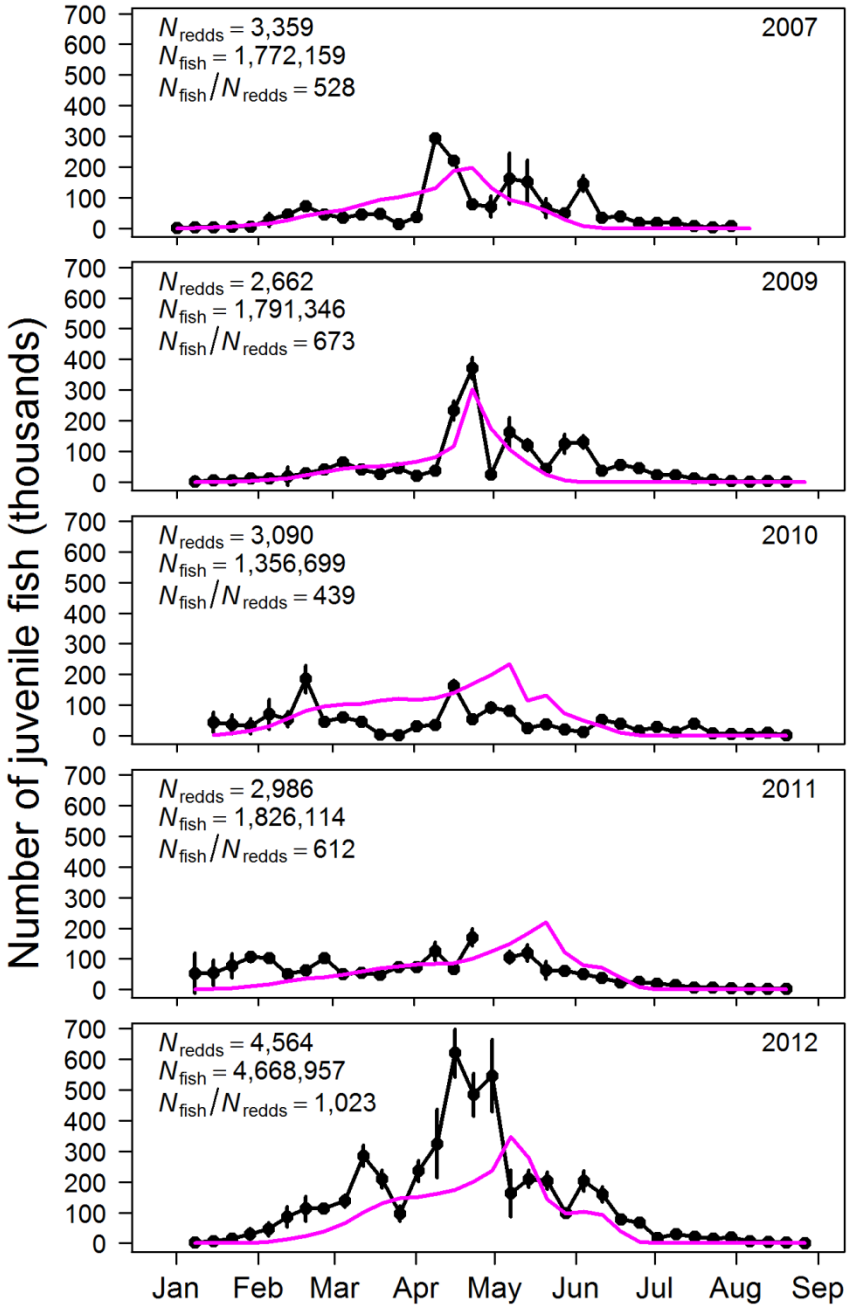

Figure 19. Annual timeseries of weekly natural-origin juvenile Chinook Salmon abundance passing Pear Tree Gulch, estimated (black) and simulated (pink). Annotated statistics include N_{redds}, the number of observed redds used to initialize the model; N_{fish}, the estimated total juvenile abundance (sum of all weeks); and the ratio of estimated abundance to the observed redd abundance (i.e., the mean number of juveniles per redd). Error bars show ± 1 SD of the original point estimate unadjusted for the overwintered portion of the juvenile population excluded for model calibration.

Simulated and Estimated Migration Timing

To compare migration timing between simulated and estimated abundance, we identified dates marking when the 20th, 50th, and 80th percentile of each outmigrant population passing Pear Tree Gulch. The onset of the migration period for natural-origin fish (i.e., the 20th percentile of arrivals at the Pear Tree trap) from trap abundance estimates were more variable than S3 simulations. However, interannual variation in the peak (50th percentile) and tail (80th percentile) of the migration period showed substantially less variation between both estimated and simulated abundance. For observed abundance estimates of natural-origin fish, the beginning of the migration period ranged from February 5 to April 9, a span of 8 weeks (table 7, figs. 20, 22–23). In contrast, the beginning of the migration period for S3 simulations ranged from March 12 to 26, a span of only 2 weeks. Deviations between the simulated and estimated migration onset were, at most, 7 weeks apart. For natural-origin fish, the simulated peak migration time occurred an average of about 11.2 days later than the observed peak. The length of the natural migration period (from the 20th to the 80th percentile) was more compressed for S3 simulations, averaging 49.0 and 67.2 days for simulated and observed juveniles, respectively. The end of the migration period, as measured by 80 percent of the run having migrated, was better simulated. Deviations between simulated and observed estimates were within 1 week on average, but occurred up to 4 weeks earlier. It is important to note that the trap-based summaries of run timing are based on values that are, like all statistics, inherently uncertain.

Compared to the natural-origin population, hatchery fish arrived later, over a much more compressed time-frame, and exhibited little interannual variation in migration timing (figs. 20–21, 23). Simulations matched estimated hatchery migration timing very well. The average length of the hatchery migration period was 11.2 and 18.2 days for simulated and trap-based estimates, respectively (table 7). Overall, the S3 model performed reasonably well at matching the beginning, peak, and tail ends of the estimated migration period for both natural and hatchery source populations.

Table 7. Dates for the 20th, 50th, and 80th percentiles of natural- and hatchery-origin source populations arriving at Pear Tree Gulch based on simulated and estimated weekly juvenile Chinook Salmon abundance.

	Trap-based estimate			Simulated		
Year	20th	50th	80th	20th	50th	80th
			Natural origin			
2007	26 March	16 April	21 May	19 March	16 April	30 April
2009	9 April	23 April	28 May	26 March	23 April	30 April
2010	19 February	9 April	7 May	12 March	16 April	7 May
2011	5 February	2 April	14 May	26 March	7 May	28 May
2012	19 March	16 April	14 May	26 March	30 April	14 May
			Hatchery origin			
2007	4 June	4 June	11 June	11 June	11 June	18 June
2009	4 June	18 June	2 July	4 June	11 June	18 June
2010	4 June	11 June	18 June	4 June	4 June	11 June
2011	28 May	11 June	18 June	11 June	18 June	25 June
2012	4 June	11 June	25 June	11 June	18 June	25 June

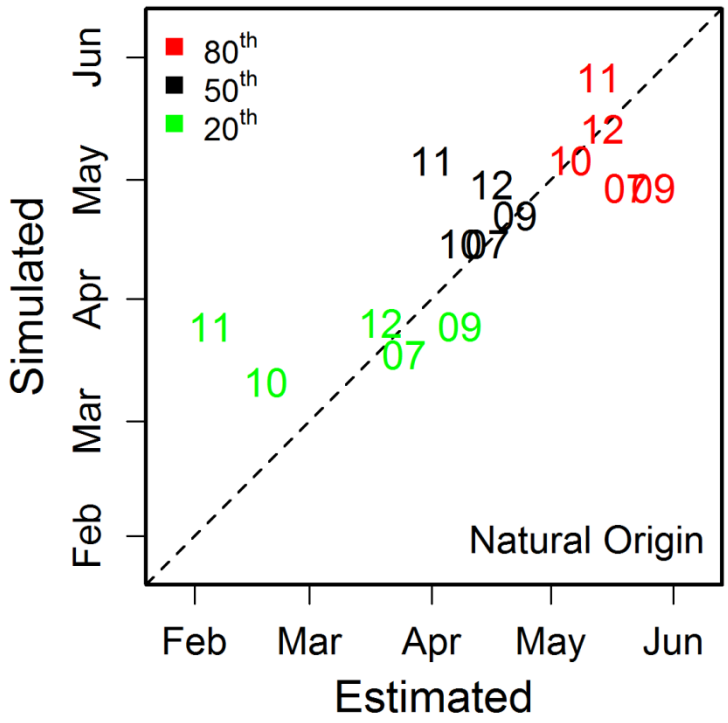

Figure 20. Simulated and estimated run timing of natural-origin juvenile Chinook Salmon passing Pear Tree Gulch (rkm 117.9), Trinity River, California. Scatter representing the 20th, 50th, and 80th percentiles of the run are labeled according to the last two digits of the outmigrant year. The dashed line shows the 1:1 line where percentiles from simulations equals percentiles from estimated abundance.

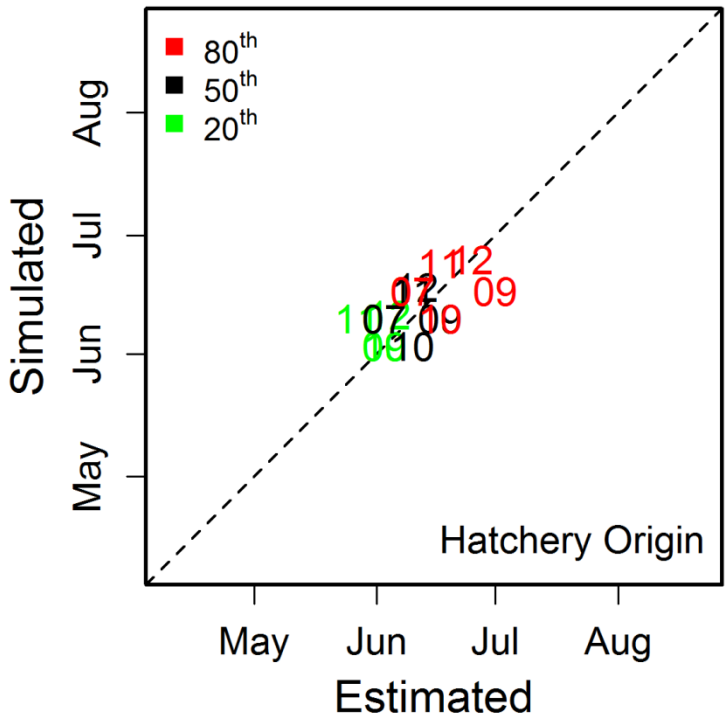

Figure 21. Simulated and estimated run timing of hatchery-origin juvenile Chinook Salmon passing Pear Tree Gulch (rkm 117.9), Trinity River, California. Scatter representing the 20th, 50th, and 80th percentiles of the run are labeled according to the last two digits of the outmigrant year. The dashed line shows the 1:1 line where percentiles from simulations equals percentiles from estimated abundance.

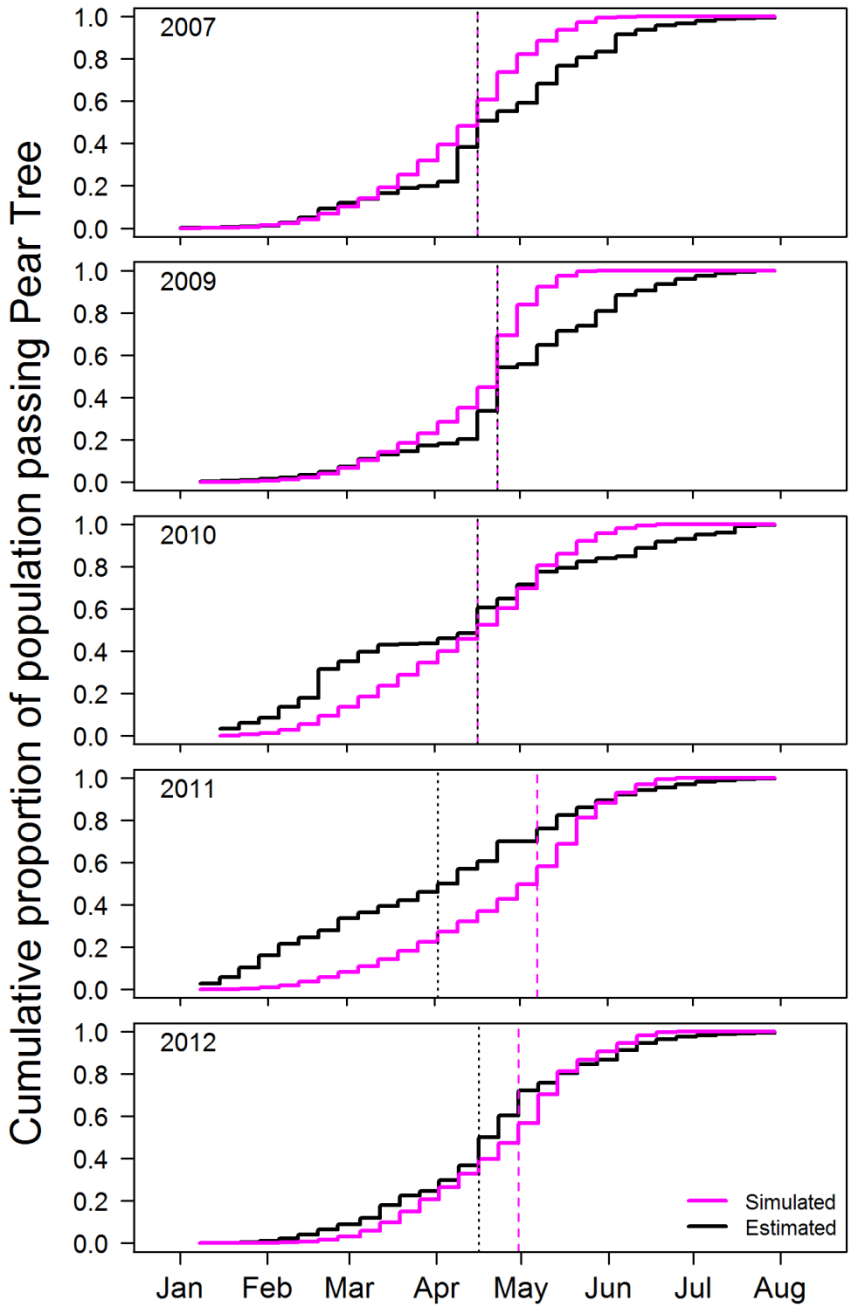

Figure 22. Outmigrant timing of natural-origin juvenile Chinook Salmon passing Pear Tree Gulch during the 5 calibration years, Trinity River, California. Step-plots show the cumulative weekly proportion of the total migrating population, estimated (black) and simulated (pink). Vertical dotted and dashed lines show the date when half of the population, estimated and simulated, respectively, had passed Pear Tree Gulch.

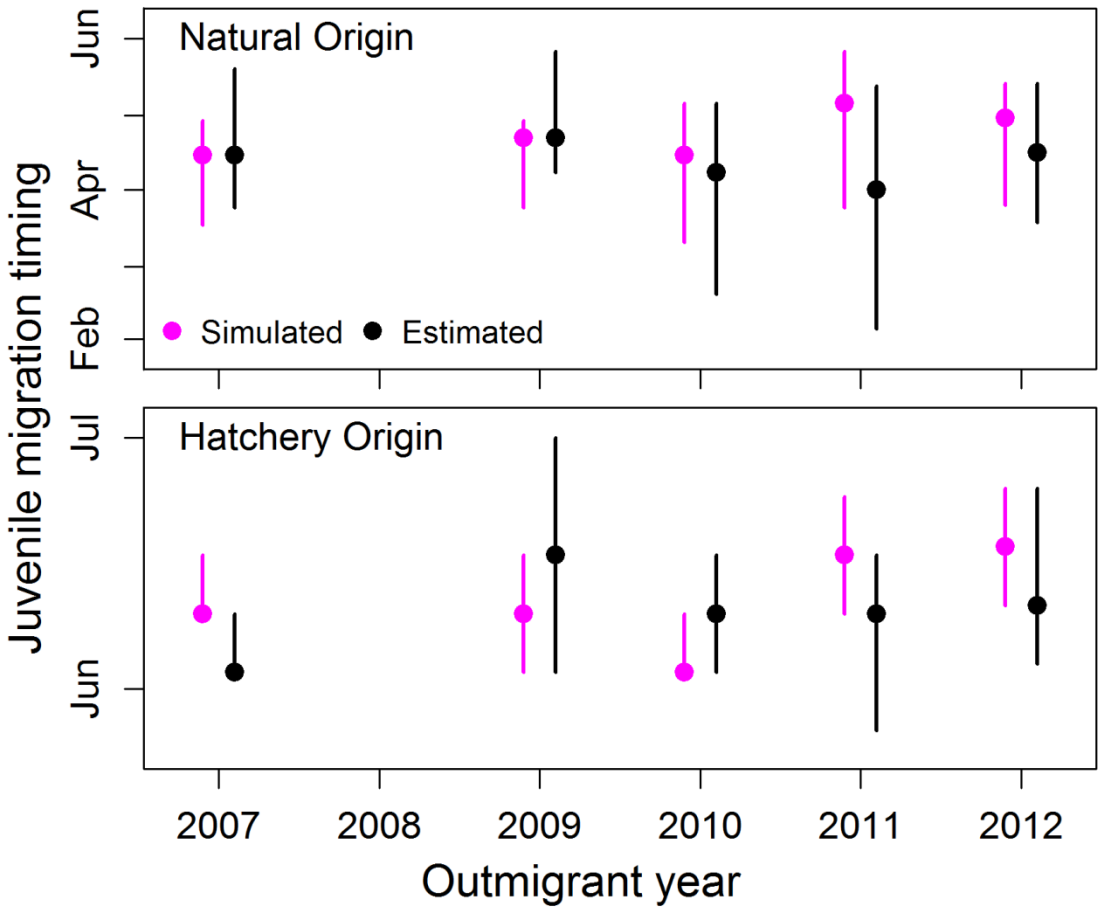

Figure 23. Simulated and estimated run-timing of natural- and hatchery-origin juvenile Chinook Salmon passing Pear Tree Gulch (rkm 117.9), Trinity River, California. Solid circles show the median and whiskers display the 20th–80th percentiles of the run.

Size of Outmigrants at Pear Tree Gulch

We evaluated the performance of the growth model component of S3 by comparing simulated and observed fork-lengths at Pear Tree Gulch. Simulated weekly mean fork-lengths of fish arriving at Pear Tree Gulch were compared to empirical measurements of individuals captured in the trap for each of the 5 calibration years (fig. 24). Early on during the migration period, from January to May, fork-lengths of the simulated natural-origin Spring and Fall Chinook Salmon populations appear to substantially underestimate the observed size of fish caught in the trap. Because screw traps sample in the thalweg, these traps may be less likely to capture fry-sized fish moving close to shore, which could be causing the disagreement between simulated and observed size. From May to July, simulated size match the observed fork-lengths reasonably well. Generally, simulated hatchery-origin fish were larger than their natural-origin counterparts, and Spring Chinook were larger than Fall Chinook Salmon. Growth trajectories were relatively flat from January through March. Beginning in April, growth trajectories substantially increase indicating an onset of accelerated growth. In early to mid-May, the mean size of naturally spawned fish transition from fry to parr. The natural-origin populations had all passed Pear Tree Gulch prior to their weekly mean fork-lengths transitioning to smolt-size.

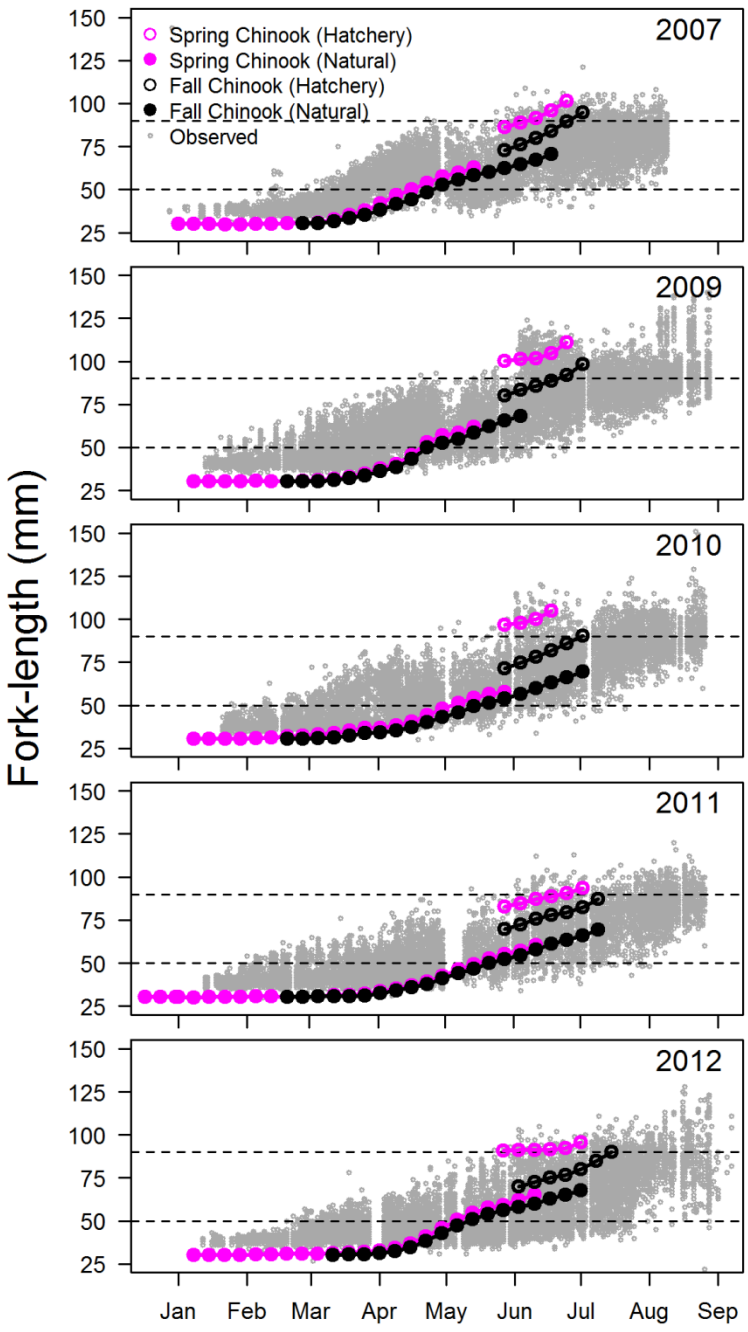

Figure 24. Weekly mean fork-lengths of simulated fish passing Pear Tree Gulch, and daily empirical measurements of individuals sampled at the trap, plotted for the 5 calibration years. Simulated weekly means are summarized for each of the four sub-populations, Spring and Fall Chinook Salmon of natural- and hatchery-origin. Dashed lines show the fork-length size cutoffs for categorizing fry, parr, and smolt age-classes.

Discussion

In this report, we constructed and parameterized the S3 as the fish production model to support the Trinity River decision support system (DSS). The structure of S3 makes it a particularly useful fish production model for the DSS because population dynamics are sensitive to (1) water temperature, (2) daily flow management, and (3) habitat quality and quantity. Each of these variables are key management parameters under consideration in the Trinity River Restoration Program. Furthermore, the Trinity River S3 model is unique and unprecedented among detailed simulation models of fish populations owing to (1) state-of-the-art sub-models forming key drivers in S3 (e.g., hydrodynamics and fish habitat models), (2) high-quality abundance estimates available for evaluating model output, (3) calibration of the model to estimate key demographic parameters, and (4) comparison of alternative hypotheses about the mechanisms of density-dependence driving population dynamics.

Inputs for the Trinity River S3 model were constructed from state-of-the-art models of spatially explicit hydrodynamics (Bradley, 2016) and quantitative fish habitat relationships (Som and others, 2017). Because of their complexity and computational burden, two-dimensional hydrodynamic models typically focus on modeling relatively short reaches of river (e.g., hundreds of meters). For example, the Klamath River S3 model relied on 2D hydrodynamic models for eight reaches throughout the Klamath River, which required extrapolating habitat quantity from the 2D models to un-modeled reaches (Perry and others, 2018b). In contrast, the SRH-2D model was applied to the entire 40-mile Restoration Reach, providing two-dimensional hydrodynamic output for every MHU in the S3 model. Thus, extrapolation from modeled to un-modeled habitat units was unnecessary. One tradeoff of constructing a hydrodynamic model for the entire 40-mile Restoration Reach is that computational cells were larger than those from the 2D model, a characteristic required to achieve computational feasibility. During initial stages of model development, we worked closely with the SRH-2D modeling team to evaluate accuracy and precision of the model to predict water velocity, a key habitat parameter. This analysis resulted in modifications to the model to decrease cell size and increase the number of cells near the shore to obtain sufficiently accurate depth and velocity estimates for predicting juvenile habitat capacity.

We used a novel technique for estimating the habitat capacity of meso-habitat units from the output of the SRH-2D hydrodynamic model. Often, habitat quality and quantity is measured in terms of the amount of suitable habitat (e.g., square meters, acres, or hectares), which may be quantified using presence-only data with habitat suitability criteria (Som and others, 2016) or presence-absence data with logistic regression (Tiffan and others, 2006). However, standard models for density-dependence use carrying capacity, not the amount of suitable habitat. Capacity can be estimated from suitable habitat area given an estimate of the maximum density within suitable habitat. For example, Beechie and others (2015) estimated reach-level capacity of the Trinity River by assigning different fish densities to habitat categories with different suitabilities of depth, velocity, and cover. In contrast to this approach, the model developed by Som and others (2018) uses continuous measures of depth, velocity, and cover distance (i.e., not categorized) to estimate the expected distribution of fish density given the predicted mean fish density and the estimated spatial and temporal variation in density. Given that we define capacity as the upper bound for the number of fish that a habitat unit can hold, we estimate capacity as the 95th percentile of the distribution of fish density, as predicted by the habitat covariates.

Because we developed a new method for estimating capacity, we evaluated whether capacity estimates generated by the model were consistent with expectations based on knowledge about competition for space. It is important to note that the capacity model we used was fit to snorkel count data collected in the Trinity River. Because density estimates are derived from "instantaneous" snorkel counts of fish, capacity estimates should be thought of as the maximum density of fish that can occupy a given habitat at a given instant in time (e.g., on a given day). From this definition, it reasons that competition for space, food, and territoriality will set an upper limit to the density that a given habitat can hold.

To evaluate our capacity model, we asked whether the predicted capacity in the "best" habitat exceeded densities that would be expected based on competition for space. We defined the "best" habitat as observed covariates that produced the highest 20 percent of predicted capacities (i.e., the 80th–100th percentile of capacity). The maximum predicted capacity based on the data collected by Som and others (2018) was 294.9 fish/m^2 for fry and 94.7 fish/m^2 for parr. For comparison, we used findings of Neuswanger and others (2016), who developed videography techniques for quantifying feeding behavior in schooling aggregations of juvenile Chinook Salmon. The authors found that individuals feeding within schools avoided each other and maintained a distance of 1.0–2.9 body lengths away from adjacent individuals. We calculated the range in fish density of fry and parr maintaining distances of 1.0–2.9 body lengths by making the simplifying assumption of equidistant spacing between fish and an average fish size of 45 mm and 65 mm for fry and parr, respectively. We found that our estimates of maximum capacity fell within the range of densities expected based on the findings of Neuswanger and others (2016; fig. 25). This comparison shows that capacity estimates from our model are consistent with expected densities when fish are maintaining feeding territories within schooling aggregations.

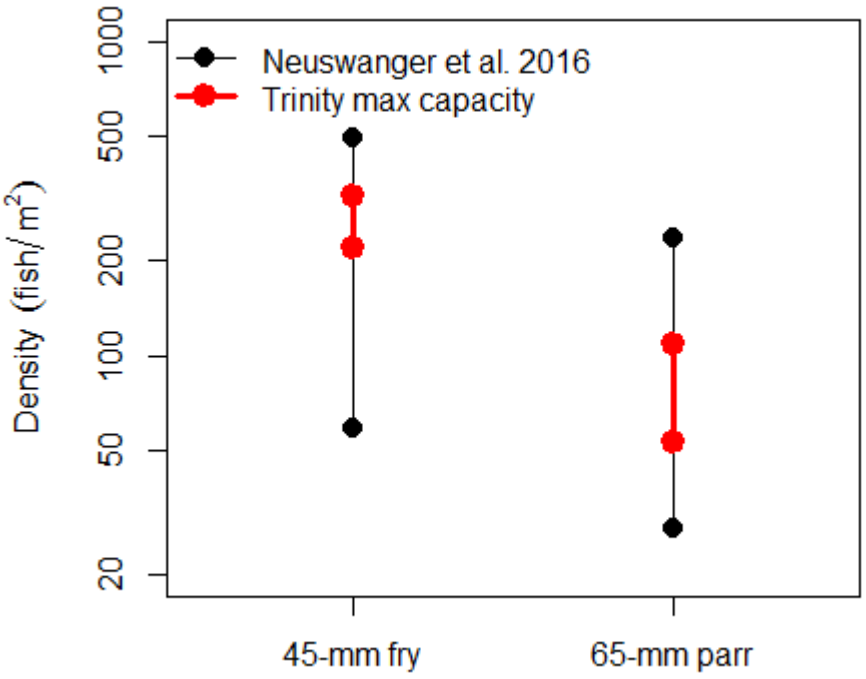

Figure 25. Comparison between maximum capacity for the Trinity River based on Som and others (2018) to expected densities for schooling juvenile Chinook Salmon based on Neuswanger and others (2016).

We identified important emergent properties of the S3 model that arose from applying the capacity model to SRH-2D output. First, we found the highest capacity in pools, followed by runs and riffles (fig. 10). These findings make biological sense, providing support for the methods and models used to generate a daily time series of MHU-specific capacity. Second, differences in capacity among habitat types affect population dynamics in S3 through the density-dependent movement function. For example, because riffles have the lowest capacity, fish occupying riffles have the highest probability of moving out of riffles relative to runs or pools (fig. 15). In turn, this movement process will cause fish to spend the least time in riffles and most time in pools. These dynamics alone provide some insight into how habitat changes might be expected to influence population dynamics. For example, increasing the amount of pool habitat while decreasing run or riffle habitat would increase capacity, which in turn would increase residence times in the Restoration Reach, shifting the run to a later emigration timing. These differences in dynamics among habitat types were not built into the model but emerge naturally from the underlying habitat structure of each computational cell in SRH-2D, how that structure is predicted to affect capacity of each computational cell, and how capacity of each cell aggregates over each habitat unit.

A key thesis underlying S3 is that river flow affects juvenile fish habitat, which in turn influences population dynamics through density-dependent mechanisms. Density dependence may manifest in either growth (Grant and Imre, 2005), movement (Hendrix and others, 2014), or survival rates (Einum and others, 2006). Therefore, we constructed the S3 modeling framework to allow density dependence to be expressed in all three demographic rates, providing the user flexibility to apply density dependence via just one mechanism, multiple mechanisms, or different mechanisms at different life stages. Clearly, the particular choice of how density dependence is structured in S3 will determine the simulated response of juvenile salmon to spatiotemporal variation in habitat capacity.

By fitting S3 to observed abundance estimates at the Pear Tree trap, we were able to evaluate whether density-dependent movement or survival produced a pattern of simulated abundance that was more consistent with observed abundance estimates. Model selection criterion favored the model with density-dependent movement over that with density-dependent survival. Furthermore, the model with density-dependent movement provided a better fit to data than did the model where all rates were density-independent. This finding provides quantitative evidence for a link between habitat and population dynamics.

The alternative models we investigated represent a small subset of possible hypotheses about how density dependence manifests in juvenile salmon populations. For example, Einum and others (2006) found that density dependence played a role in the mortality of Atlantic salmon (*Salmo salar*) fry, but as fish grew, density dependence was not expressed in mortality, but through growth and movement. This ontogenetic shift in the expression of density dependence represents one possible hypothesis that could be implemented in S3. However, implementing more complex models will likely pose challenges for parameter estimation.

The calibration technique we used is an indirect method for estimating daily demographic parameters from a multi-year time series of abundance. That is, given the assumed functional form for demographic rates, the calibration is aimed at optimizing values of movement and survival parameters that produce simulated weekly abundances that best match the pattern of observed abundance estimates. Information about movement and survival rates in the trap abundance estimates arises solely from (1) the within-year temporal pattern of weekly abundance and (2) among-year differences in outmigration timing and abundance. Through multiple iterations of calibration and sensitivity analysis, we found that movement rates and survival rates are often highly correlated (see appendix figs. 1–7). This correlation arises because different combinations of daily movement and survival rates can produce the same abundance at the Pear Tree trap. For example, if we increase daily movement rates, then abundance passing the trap increases because fish have a shorter residence time within the system, which increases survival within the Restoration Reach. Therefore, to match abundance at the trap, increases in movement rate must be accompanied by a coincident decrease in survival rate. Because of the indirect inference and correlation between movement and survival parameters, we suspect that it will be difficult to estimate parameters of more complex and potentially more realistic models by fitting to abundance data alone. For example, although a sensitivity analysis revealed that a global minimum negative log-likelihood exists to enable identifiability of both movement and survival parameters, the sensitivity of the likelihood to alternative parameter values was low, as indicated by the likelihood changing by only two units over a wide range of parameter values (see appendix figs. 1-1–1-8). This finding suggests a "ridge" in the likelihood space between movement and survival parameters due to high correlation. Therefore, the fitting of these more complex models could be improved by using estimates of demographic parameters generated outside of the calibration procedure and based on data collected independently from the trap abundances.

Although the trap-abundance estimates are a critical element of calibrating and evaluating S3, additional monitoring focused on direct estimation of movement or survival rates could substantially improve both model parameterization and our understanding of movement, growth, and survival dynamics in the Restoration Reach. For example, mark-recapture studies with individually identifiable fish would provide direct estimates of individual travel time and migration rate. Physical recapture of marked fish would provide information about individual growth rates. By combining different data sources in the calibration (e.g., abundance and mark-recapture data), mark-recapture data could be used to estimate the movement parameters, and the trap-abundance estimates would provide information about survival. Such an approach would allow us to fit more complex models and to expand the range of hypotheses that could be evaluated.

Although mark-recapture studies would provide data to parameterize S3, one challenge with mark-recapture methods is obtaining sufficient recaptures for high-precision parameter estimates. Passive Integrated Transponder (PIT) tag technology is now a common approach for studying growth, movement, and survival of juvenile salmonids. Instream antennas that continuously monitor for tags provide passive "recaptures" of tagged fish, thereby increasing recapture rates. Additionally, PIT tag size has been reduced, allowing fish as small as 45 mm to be tagged (Tiffan and others, 2015). Although PIT-tag studies have historically been limited to small streams owing to limited read range, advances in antenna technology are now making it feasible to conduct PIT tag studies on relatively large rivers such as the Trinity River (Rundio and others, 2017). A focused mark-recapture study utilizing PIT tags in the Trinity River would provide considerable additional data for parameterizing demographic rates in S3.

Given that the model was initialized with only the spatiotemporal distribution of spawners, it performed remarkably well at capturing the essential features of the outmigration that are ultimately governed by rates of growth, movement, and mortality. Overall, model predictions matched the observed timing, abundance, and size of outmigrants at the Pear Tree trap. As with any model, some aspects of model fit were imperfect—the model consistently underestimated annual peaks in weekly abundance and underestimated mean fork-length early in the outmigration season. Lack of fit can arise from multiple causes including: (1) incorrectly specified model inputs, (2) imprecise or inaccurate abundance estimates to which model outputs are compared, (3) inaccurate values of fixed parameters (those not estimated during calibration), (4) wrong model structure for demographic rates, or (5) important demographic drivers that are not included in the model.

We found that the model performed well at predicting the annual total abundance passing Pear Tree in all years except 2012 (2011 brood year; fig. 16), the year of highest spawner abundance. One potential cause of this under prediction could be underestimation of the number of spawners that contributed to juvenile production. Since 2012 was a year of high spawner abundance, two processes could have contributed to underestimation of spawners. First, as spawner abundance increases, superimposition and merging of visually identifiable redds into a "redd agglomeration" makes tracking of individual redds difficult, leading to underestimation (Groves and others, 2013). Second, as spawner abundance increases, spawners expand into territory such as tributaries that are infrequently used as spawning habitat (Thurow, 2000). Although tributary spawning is thought to represent a small fraction of total spawning upstream of the Pear Tree trap, if that fraction increases in years of high spawner abundance, then the mainstem redd counts that we used as an estimate of spawner abundance may underestimate the true number of spawners contributing to the juvenile population. Estimates of outmigrating juveniles and spawner abundances generated from TRRP monitoring programs provide some evidence for these hypotheses. For 2012, 1,023 juveniles per redd were produced, whereas in other years 443–675 juveniles per redd were produced (fig. 19). Although we cannot rule out higher-than-average survival as the cause of high productivity, 1,023 juveniles per redd and 3,000 eggs per female implies 34 percent survival from spawning to outmigration past Pear Tree, which seems unrealistically high.

Despite some lack of fit, it is important to note that all models are caricatures of reality. When calibrating S3, an important goal is to evaluate how well the model matches observed abundance and size when the model inputs are structured to match historical conditions as closely as possible. Although the model assumes that all inputs (flow, temperature, habitat capacity, spawners, juveniles) are known perfectly, all model inputs are uncertain quantities because they themselves are outputs of other models or estimates obtained from field sampling. In addition, when evaluating the model, our natural tendency is to view the trap abundance estimates as the truth against which the model is compared. Yet the observed trap abundance estimates contain considerable uncertainty, and this uncertainty should be kept in mind when evaluating model predictions. Thus, although we should always strive to improve model fit, uncertainty in both inputs and outputs, and the fact that the model itself is an abstraction of reality, virtually guarantee that a perfect model fit is unattainable.

We suspect that the mismatch in fish size early in the year (January–April) was driven by trap selectivity causing smaller fish to be under-represented in trap catches, although other factors may have contributed (e.g., assumptions about growth parameters or modeling only mean size versus variation in size). Size selectivity of the screw trap favors collection of larger individuals that are more likely to be moving in the upper water column relative to small fry that are more likely to be shoreline oriented. In our application of S3 to the Klamath River, it is worth noting that the mean size of simulated fish is similar to observed fish size both early and later in the season (Perry and others, 2018b). Trap sites on Klamath River use both screw traps and shoreline frame traps. Thus, the use of frame traps in sampling efforts on the Klamath River yield a more representative sample of fish moving both offshore and close to shore, compared to just screw traps alone on the Trinity River. That said, we cannot rule out other hypotheses.

We assumed a fixed proportion of maximum consumption of 0.66 in the Wisconsin bioenergetics model, but consumption may have been higher early in the season when fry densities are low. In the calibration, our goal was to parameterize survival and movement, hold growth parameters fixed, and then examine how well predicted size matched observed size with fixed growth parameters. We chose the value of 0.66 for consumption because (1) it matches growth rates of juvenile Chinook Salmon fed an ad libitum diet in laboratory studies (Perry and others, 2015), and (2) this is close to the value identified by Armstrong and Schindler (2011) as the average consumption across many fish taxa. An alternative model structure would be to allow the proportion of maximum consumption to vary with fish density to reflect competition for food resources. Density-dependent growth would allow fry emerging early in the season to grow faster when densities are lower, possibly providing better fit to the observed data, although implementation of an alternative model structure would benefit directly from estimates of consumption patterns over the growing season. Another potential cause of a size mismatch is that the model keeps track of only the mean mass of fish in each life stage, and not individuals. As fry continually emerge at a mass of 0.3 g from January through April, they mix with previously emerged fry, reducing the mean mass of the fry life stage. As emergence of Fall Chinook Salmon ceases in April, mean mass begins to quickly increase partially owing to lack of newly emerged fry reducing the average mass of fry.

In constructing this first version model, we made many decisions about model structure and which demographic drivers to include or exclude. Recognizing that the baseline structure of S3 is already complex, our goal was to keep the model as simple as possible by including the minimal amount of structure required to emulate observed population dynamics. For example, although redd scour is an important process driving egg mortality, we elected to leave this process out of the first version of the model because (1) more work is needed to develop a detailed scour model that fits within the S3 framework and accurately captures this process in the Trinity River, and (2) high flows likely to scour redds were absent in the brood years we used for calibrating the model. As another example, predation by brown trout and rainbow trout is an important mortality mechanism in the Trinity River (Naman, 2008; Alvarez, 2017). Although we have constructed a predator-prey sub-model that would allow predation rates to vary spatially in the Restoration Reach, we elected not to implement this model for the first version because it requires spatially explicit information about predator densities. Furthermore, because primary management decisions revolve around flow management, habitat restoration, and temperature, it was paramount to focus the model structure on these variables.

During a review of the TRRP's first phase of restoration activities, the TRRP Science Advisory Board (SAB) recommended the TRRP immediately focus on implementation of a Decision Support System (DSS), and noted development of the DSS's core elements as the highest priority of the TRRP (Buffington and others, 2014). The habitat and S3 models described in this report are both core elements of the DSS, and their application will help provide valuable information to TRRP scientists and decision makers. For smaller spatial scales (e.g., an individual restoration site), one would not expect a full population dynamics model, nor the entire fish population of study, to be measurably sensitive to alterations or changes. However, the habitat model could be employed to evaluate how differing restoration alternatives alter the capacity of the site, and help predict which restoration design provides the greatest increases in capacity across flows.

The S3 model offers the opportunity to integrate biological and physical characteristics over the entire temporal and spatial freshwater residency of juvenile salmonid populations. As such, the S3 model will provide valuable insights into the potentially variable impacts that various management decisions will have in the Trinity River. Combinations of system attributes (e.g., physical habitat, hydrographs) subject to manipulation by managers can be translated into scenarios that form the inputs for S3 model runs. The S3 model will provide predictions of the relative differences of population demographics such as fish abundance, size, and run timing across these scenarios. These predictions will in turn inform the broader DSS, help complete the adaptive management loop, and lead to a refined management decision process for the benefit of the Trinity River.

Acknowledgements

This work was funded by Interagency Grant number 4500064515 from the U.S. Fish and Wildlife Service to the U.S. Geological Survey. This research was facilitated by high-performance computing resources provided by the Core Science Analytics, Synthesis, & Libraries (CSASL) Advanced Research Computing (ARC) group at the U.S. Geological Survey. We are grateful to staff of multiple State, Federal, and Tribal agencies who have collected the field data on which our modeling efforts are based. We are grateful to our late co-author, colleague, and friend Edward (Ted) Jones. Ted spent many years roaming the Trinity River. As such, this research project was near and dear to his heart.

References Cited

Alvarez, J.S., 2017, Abundance, growth, and predation by non-native brown trout in the Trinity River, California: Masters Thesis, Humboldt State University, 60 p., accessed October 1, 2018, at http://digitalcommons.humboldt.edu/etd/47.

Armstrong, J.B., and Schindler, D.E., 2011, Excess digestive capacity in predators reflects a life of feast and famine: Nature, v. 476, no. 7358, p. 84–88, accessed October 1, 2018, at https://doi.org/10.1038/nature10240.

Bartholow, J.M., 1996, Sensitivity of a salmon population model to alternative formulations and initial conditions: Ecological Modelling, v. 88, no. 1–3, p. 215–226, accessed October 1, 2018, at https://doi.org/10.1016/0304-3800(95)00108-5.

Bartholow, J.M., Laake, J.L., Stalnaker, C.B., and Williamson, S.C., 1993, A salmonid population model with emphasis on habitat limitations: Rivers, v. 4, no. 4, p. 265–279.

Bartholow, J., Heasley, J., Laake, J., Sandelin, J., Coughlan, B.A.K., and Moos, A., 2002, SALMOD—A population model for salmonids—User's manual (Version W3): U.S. Geological Survey, 76 p.

Beechie, T.J., Pess, G.R., Imaki, H., Martin, A., Alvarez, J., and Goodman, D.H., 2015, Comparison of potential increases in juvenile salmonid rearing habitat capacity among alternative restoration scenarios, Trinity River, California: Restoration Ecology, v. 23, no. 1, p. 75–84, accessed October 1, 2018, at https://doi.org/10.1111/rec.12131.

Borok, S., Cannata, S., Hill, A., Hileman, J., and Kier, M.C., 2014, Annual report, Trinity River Basin salmon and steelhead monitoring project, 2011–2012 season: California Department of Fish and Wildlife.

Bradley, D.N., 2016, Trinity River 40 Mile Hydraulic Model—Development and analysis. Report to the Trinity River Restoration Program (TRRP), Technical Service Center report no SRH-2016-27: Denver, Colorado, U.S. Bureau of Reclamation.

Buffington, J., Jordan, C., Merigliano, M., Peterson, J., and Stalnaker, C., 2014, Review of the Trinity River Restoration Program following Phase 1, with emphasis on the Program's channel rehabilitation strategy: Prepared by the Trinity River Restoration Program's Science Advisory Board for the Trinity River Restoration Program with assistance from Anchor QEA, LLC, Stillwater Sciences, BioAnalysts, Inc., and Hinrichsen Environmental Services.

Burnham, K.P., and Anderson, D.R., 2002, Model selection and multimodel inference—A practical information-theoretic approach: New York, Springer.

Chamberlain, C.D., Quinn, S., and Matilton, W., 2012, Distribution and abundance of Chinook Salmon redds in the mainstem Trinity River 2002 to 2011: U.S. Fish and Wildlife Service, Arcata Fisheries Technical Report TR 2012-16.

David, A.T., 2017, Klamath and Trinity River intra-gravel water temperatures, 2015 and 2016: U.S. Fish and Wildlife Service, Arcata Fisheries Data Series Report Number DS 2017-49.

Deriso, R.B., Maunder, M.N., and Skalski, J.R., 2007, 2007, Variance estimation in integrated assessment models and its importance for hypothesis testing: Canadian Journal of Fisheries and Aquatic Sciences, v. 64, no. 2, p. 187–197, accessed October 1, 2018, at https://doi.org/10.1139/f06-178.

Einum, S., Sundt-Hansen, L., and Nislow, K.H., 2006, The partitioning of density-dependent dispersal, growth and survival throughout ontogeny in a highly fecund organism: Oikos, v. 113, p. 489–496, accessed October 1, 2018, at https://doi.org/10.1111/j.2006.0030-1299.14806.x.

Geist, D.R., Abernethy, S.C., Hand, K.D., Cullinan, V.I., Chandler, J.A., and Groves, P.A., 2006, Survival, development, and growth of Fall Chinook Salmon embryos, alevins, and fry exposed to variable thermal and dissolved oxygen regimes: Transactions of the American Fisheries Society, v. 135, no. 6, p. 1462–1477.

Goodman, D.H., Som, N.A., Hetrick, N.J., 2018, Increasing the availability and spatial variation of spawning habitats through ascending baseflows: River Research and Applications, v. 34, p. 844–853, accessed October 3, 2018, at https://onlinelibrary.wiley.com/doi/abs/10.1002/rra.3302.

Grant, J.W.A., and Imre, I., 2005, Patterns of density-dependent growth in juvenile stream-dwelling salmonids: Journal of Fish Biology, v. 67, p. 100–110, accessed October 1, 2018, at https://doi.org/10.1111/j.0022-1112.2005.00916.x.

Groves, P.A., Chandler, J.A., Alcorn, B., Richter, T.J., Connor, W.P., Garcia, A.P., and Bradbury, S.M., 2013, Evaluating salmon spawning habitat capacity using redd survey data: North American Journal of Fisheries Management, v. 33, no. 4, p. 707–716, accessed October 1, 2018, at https://doi.org/10.1080/02755947.2013.793628.

Hendrix, N., Criss, A., Danner, E., Greene, C.M., Imaki, H., Pike, A., and Lindley, S.T., 2014, Life cycle modeling framework for Sacramento River winter run Chinook Salmon: National Oceanic and Atmopsheric Administration Technical Memorandum NOAA-TM-NMFS-SWFSC-530, 30 p., accessed October 1, 2018, at https://swfsc.noaa.gov/publications/TM/SWFSC/NOAA-TM-NMFS-SWFSC-530.pdf.

Jones, E.C., Perry, R.W., Risley, J.C., Som, N.A., and Hetrick, N.J., 2016, Construction, calibration, and validation of the RBM10 water temperature model for the Trinity River, northern California: U.S. Geological Survey Open-File Report 2016–1056, 46 p., accessed October 1, 2018, at https://doi.org/10.3133/ofr20161056.

Lai, Y.G., 2008, SRH-2D Version 2—Theory and user's manual: Bureau of Reclamation, 101 p.

Lai, Y.G., 2010, Two-dimensional depth-averaged flow modeling with an unstructured hybrid mesh: Journal of Hydraulic Engineering, v. 136, no. 1, p. 12–23, accessed October 1, 2018, at https://doi.org/10.1061/(ASCE)HY.1943-7900.0000134.

Lai, Y.G., and Greimnann, B.P., 2010, Predicting contraction scour with a two-dimensional depth-averaged model: Journal of Hydraulic Research, v. 48, no. 3, p. 383–387, https://doi.org/10.1080/00221686.2010.481846.

Manhard, C.V., Som, N.A., Perry, R.W., and Plumb, J.M., 2018, A laboratory calibrated model of coho salmon growth with utility for ecological analyses: Canadian Journal of Fisheries and Aquatic Sciences, v. 75, no. 5, p. 682–690, accessed October 1, 2018, at https://doi.org/10.1139/cjfas-2016-0506.

Naman, S.W., 2008, Predation by hatchery Steelhead on natural Salmon fry in the upper-Trinity River, California: Masters Thesis, Humboldt State University, Arcata, 66 p., accessed October 1, 2018, at humboldt-dspace.calstate.edu/xmlui/handle/2148/449.

Neuswanger, J.R., Wipfli, M.S., Rosenberger, A.E., and Hughes, N.F., 2016, Measuring fish and their physical habitats—Versatile 2D and 3D video techniques with user-friendly software: Canadian Journal of Fisheries and Aquatic Sciences, v. 73, no. 12, p. 1861–1873, accessed October 1, 2018, at https://doi.org/10.1139/cjfas-2016-0010.

Perry, R.W., Plumb, J.M., and Huntington, C.W., 2015, Using a laboratory-based growth model to estimate mass-and temperature-dependent growth parameters across populations of juvenile Chinook Salmon: Transactions of the American Fisheries Society, v. 144, no. 2, p. 331–336, accessed October 1, 2018, at https://doi.org/10.1080/00028487.2014.996667.

Perry, R.W., Plumb, J.M., Jones, E.C., Som, N.A., Hetrick, N.J., and Hardy, T.B., 2018a, Model structure of the stream salmonid simulator (S3)—A dynamic model for simulating growth, movement, and survival of juvenile salmonids: U.S. Geological Survey Open-File Report 2018-1056, 32 p., accessed October 1, 2018, at https://doi.org/10.3133/ofr20181056.

Perry, R.W., Plumb, J.M., Jones, E.C., Som, N.A., Hetrick, N.J., and Hardy, T.B., 2018b, Application of the Stream Salmonid Simulator (S3) to Klamath River Fall Chinook Salmon: U.S. Geological Survey Open-File Report 2018-1056, 32 p.

Perry, R.W., Risley, J.C., Brewer, S.J., Jones, E.C., and Rondorf, D.W., 2011, Simulating daily water temperatures of the Klamath River under dam removal and climate change scenarios: U.S. Geological Survey Open-File Report 2011–1243, 78 p., accessed October 1, 2018, at https://doi.org/10.3133/ofr20111243.

Pinnix, W.D., De Juilio, K., Petros, P., and Som, N.A., 2016, Feasibility of snorkel surveys for determining relative abundance and habitat associations of juvenile Chinook Salmon on the mainstem Trinity River, California: Yurok Tribal Fisheries Program, Hoopa Valley Tribal Fisheries Department, U. S. Fish and Wildlife Service, and Arcata Fish and Wildlife Office, Arcata Fisheries Technical Series Report Number TR 2016-24.

Plumb, J.M., and Moffitt, C.M., 2015, Re-estimating temperature-dependent consumption parameters in bioenergetics models for juvenile Chinook Salmon: Transactions of the American Fisheries Society, v. 144, no. 2, p. 323–330, accessed October 1, 2018, at https://doi.org/10.1080/00028487.2014.986336.

Plumb, J.M., 2012, Evaluation of models and the factors affecting the migration and growh of naturally-produced subyearling Fall Chinook Salmon (Oncorhynchus tshawytscha) in the lower Snake River: Doctoral Dissertation, Moscow, Idaho, University of Idaho.

R Core Team, 2017, R—A language and environment for statistical computing: Vienna, Austria, R Foundation for Statistical Computing, accessed October 1, 2018, at https://www.R-project.org/.

Rundio, D.E., Montgomery, A.N., Nesbit, M.G., Morris, M.S., Brooks, G.T., Axel, G.A., Lamb, J.J., Zabel, R.W., Ferguson, J.W., and Lindley, S.T., 2017, Central Valley passive integrated transponder (PIT) tag array feasibility study: National Oceanic and Atmospheric Administration technical memorandum NMFS, NOAA-TM-NMFS-SWFSC-573, 130 p.

Som, N.A., Goodman, D.H., Perry, R.W., and Hardy, T.B., 2016, Habitat suitability criteria via parametric distributions—Estimation, model selection and uncertainty: River Research and Applications, v. 32, no. 5, p. 1128–1137, accessed October 1, 2018, at https://doi.org/10.1002/rra.2900.

Som, N.A., Perry, R.W., Jones, E.C., De Juilio, K., Petros, P., Pinnix, W.D., and Rupert, D.L., 2018, N-mix for fish—Estimating riverine salmonid habitat selection via N-mixture models: Canadian Journal of Fisheries and Aquatic Sciences, v. 75, no. 7, p. 1048–1058, accessed October 1, 2018, at https://doi.org/10.1139/cjfas-2017-0027.

Thurow, R.F., 2000, Dynamics of Chinook Salmon populations within Idaho's Frank Church Wilderness—Implications for persistence: U.S. Forest Service Proceedings RMRS-P-15, v. 3, p. 143-151, accessed October 1, 2018, at http://www.wilderness.net/library/documents/Thurow_3-19.pdf.

Tiffan, K.F., Clark, L.O., Garland, R.D., and Rondorf, D.W., 2006, Variables influencing the presence of subyearling Fall Chinook Salmon in shoreline habitats of the Hanford Reach, Columbia River: North American Journal of Fisheries Management, v. 26, no. 2, p. 351–360, accessed October 1, 2018, at https://doi.org/10.1577/M04-161.1.

Tiffan, K.F., Perry, R.W., Connor, W.P., Mullins, F.L., Rabe, C.D., and Nelson, D.D., 2015, Survival, growth, and tag retention in age-0 Chinook Salmon: North American Journal of Fisheries Management, v. 35, no. 4, p. 845–852, accessed October 1, 2018, at https://doi.org/10.1080/02755947.2015.1052163.

Trinity River Restoration Program and ESSA Technologies, Ltd., 2009, Integrated assessment plan, version 1.0–September 2009: Weaverville, California, Draft report prepared for the Trinity River Restoration Program, 285 p.

Williamson, S.C., Bartholow, J.M., and Stalnaker, C.B., 1993, Conceptual model for quantifying pre-smolt production from flow-dependent physical habitat and water temperature—Regulated Rivers: Research and Management, v. 8, no. 1–2, p. 15–28, accessed October 1, 2018, at https://doi.org/10.1002/rrr.3450080106.

U.S. Department of Interior, 2000, Record of decision—Trinity River mainstem fishery restoration final environmental impact statement/environmental impact report. Decision by the U.S. Department of Interior, December 2000.

U.S. Fish and Wildlife Service and Hoopa Valley Tribe, 1999, Trinity River flow evaluation—Final report: U.S. Fish and Wildlife Service and Hoopa Valley Tribe, Report to the Secretary of the U.S. Department of the Interior.

U.S. Fish and Wildlife Service, Bureau of Reclamation, Hoopa Valley Tribe, and Trinity County, 2000, Trinity River mainstem fishery restoration: U.S. Department of the Interior, Final Environmental Impact Statement/Environmental Impact Report:

Zabel, R.W., and Anderson, J.J., 1997, A model of the travel time of migrating juvenile salmon, with an application to Snake River Spring Chinook Salmon: North American Journal of Fisheries Management, v. 17, no. 1, p. 93–100, accessed October 1, 2018, at https://doi.org/10.1577/1548-8675(1997)017<0093:AMOTTT>2.3.CO;2.

Zabel, R.W., 2002, Using “travel time” data to characterize the behavior of migrating animals: American Naturalist, v. 159, no. 4, p. 372–387.

Appendix 1. Supplemental Table and Figures

Table 1-1. Mean and standard deviation of observed explanatory variables used to standardize the covariates used when fitting the N-mixture model to fry and parr snorkel count data, Trinity River, California.
[SD, standard deviation]

Variable	Mean	SD
Depth (feet)	1.87	1.095
Velocity (feet per second)	1.00	0.865
Distance to cover (feet)	14.45	24.619

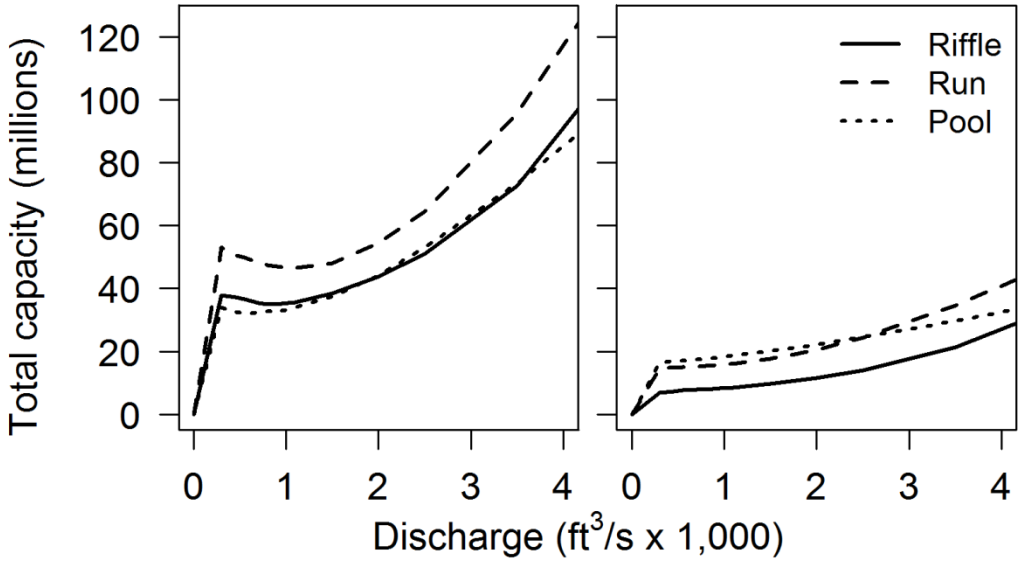

Figure 1-1. Total fry- and parr-carrying capacity for the Trinity River Restoration Reach as a function of streamflow up to 4,000 cubic feet per second (ft^3/s). Capacities were summed by meso-habitat type (riffle, run, and pool) to show relative differences in total capacity as a function of flow.

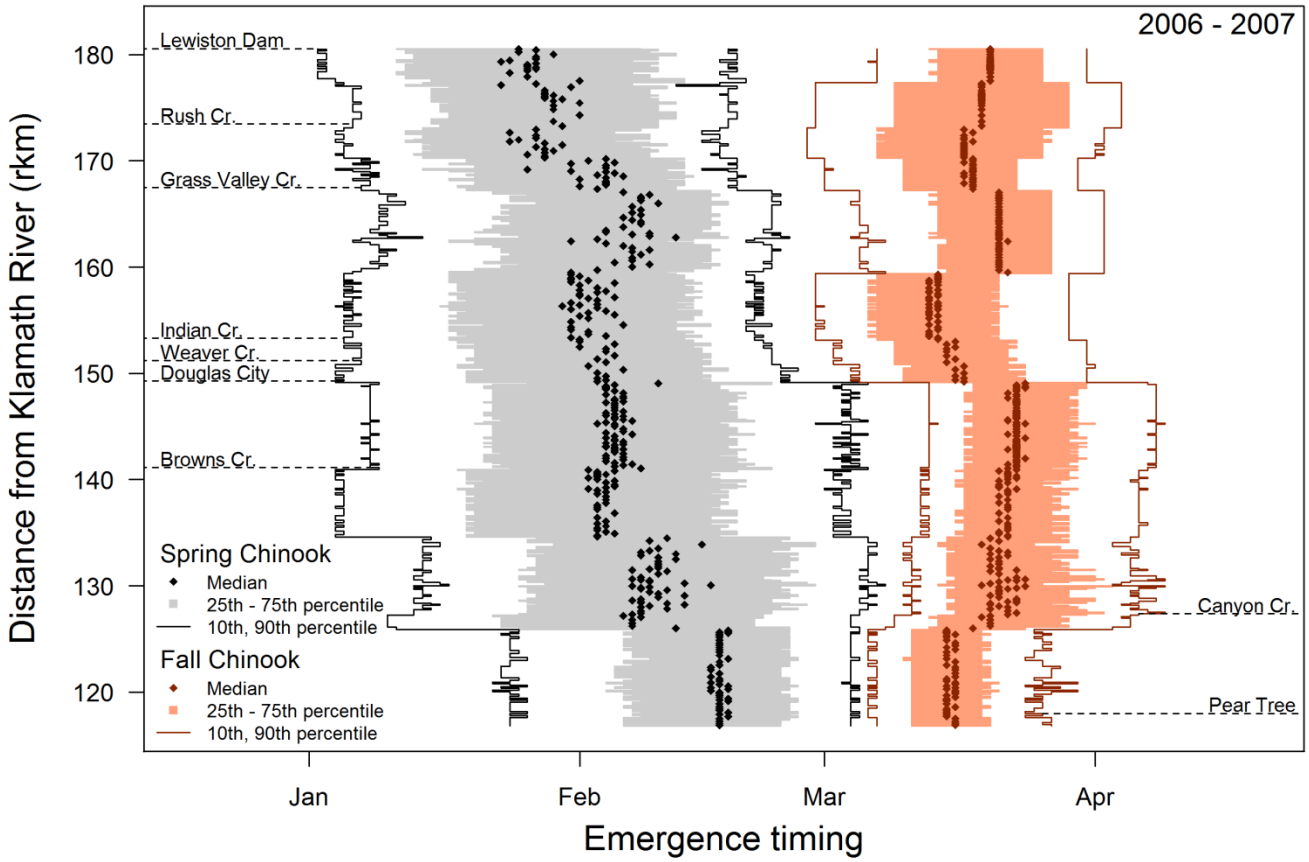

Figure 1-2. Graph showing the spatial and temporal distribution of natural-origin Spring and Fall Chinook Salmon fry emergence simulated from empirical spawner survey data, Trinity River Restoration Reach, California, 2006–07. For each of the 356 meso-habitat units, thin lines (black and red) bound dates of the 10th and 90th percentiles of simulated fry emergence, horizontal bars (gray and orange) show the 25th–75th percentile range, and diamonds (black and red) show the median (i.e., the date when half of the fry population has emerged).

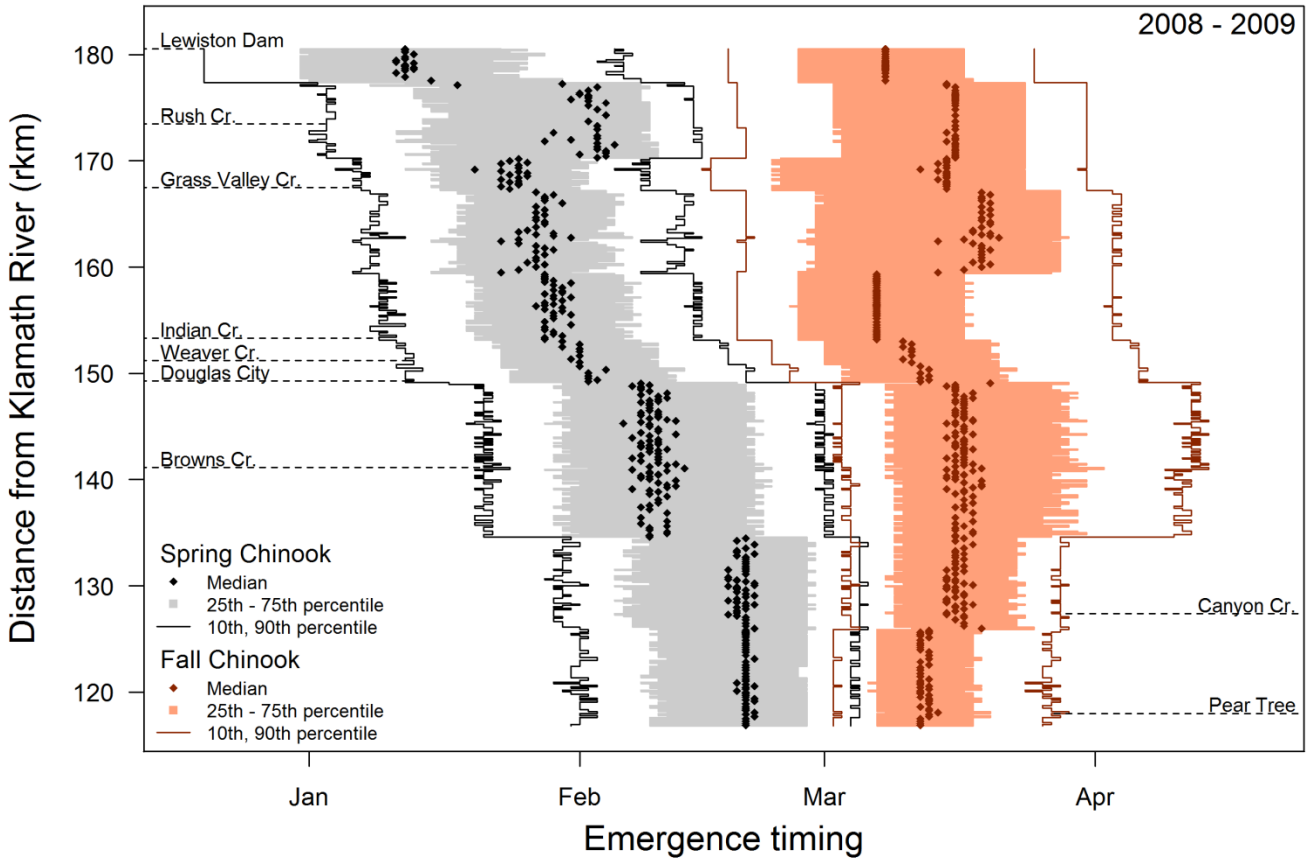

Figure 1-3. Graph showing the spatial and temporal distribution of natural-origin Spring and Fall Chinook Salmon fry emergence simulated from empirical spawner survey data, Trinity River Restoration Reach, California, 2008–09. For each of the 356 meso-habitat units, thin lines (black and red) bound dates of the 10th and 90th percentiles of simulated fry emergence, horizontal bars (gray and orange) show the 25th–75th percentile range, and diamonds (black and red) show the median (i.e., the date when half of the fry population has emerged).

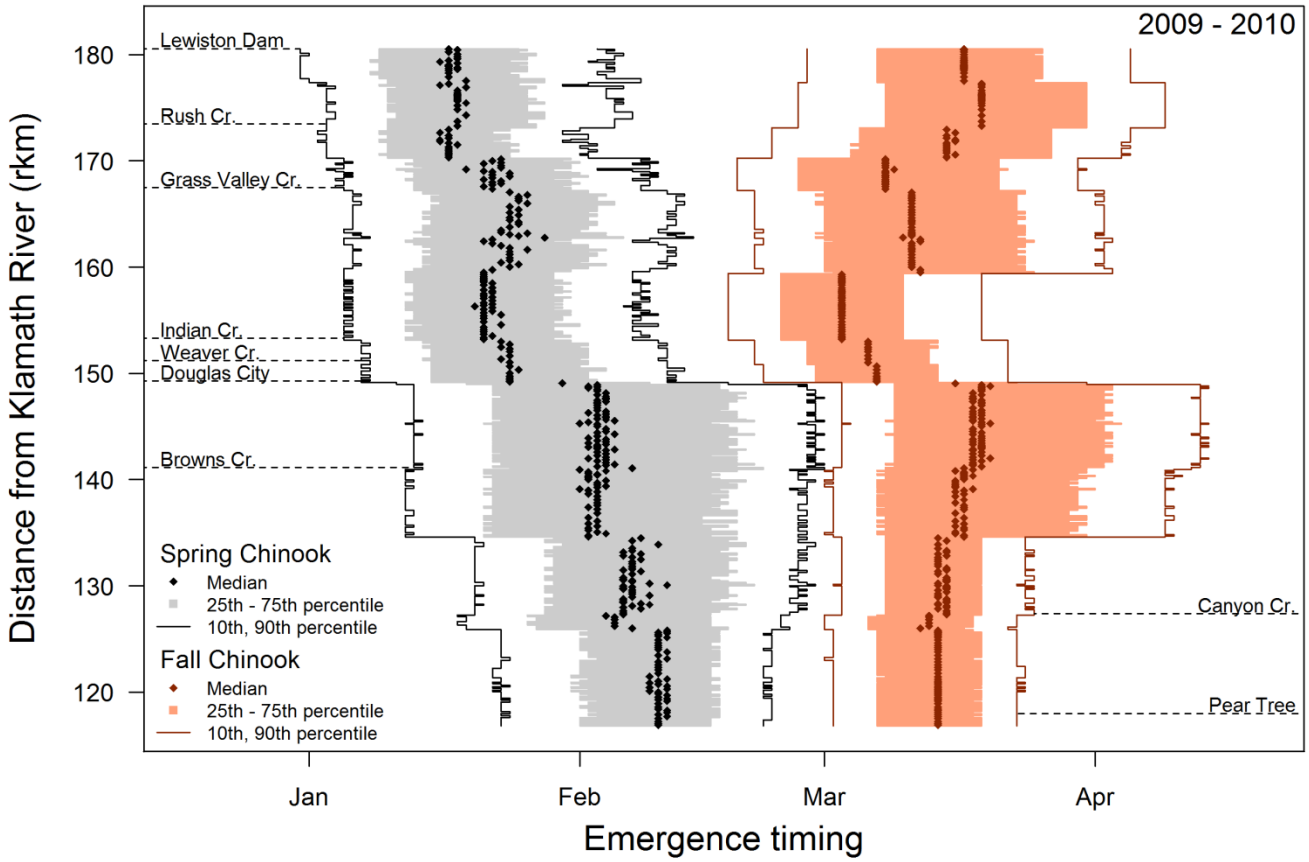

Figure 1-4. Graph showing the spatial and temporal distribution of natural-origin Spring and Fall Chinook Salmon fry emergence simulated from empirical spawner survey data, Trinity River Restoration Reach, California, 2009–10. For each of the 356 meso-habitat units, thin lines (black and red) bound dates of the 10th and 90th percentiles of simulated fry emergence, horizontal bars (gray and orange) show the 25th–75th percentile range, and diamonds (black and red) show the median (i.e., the date when half of the fry population has emerged).

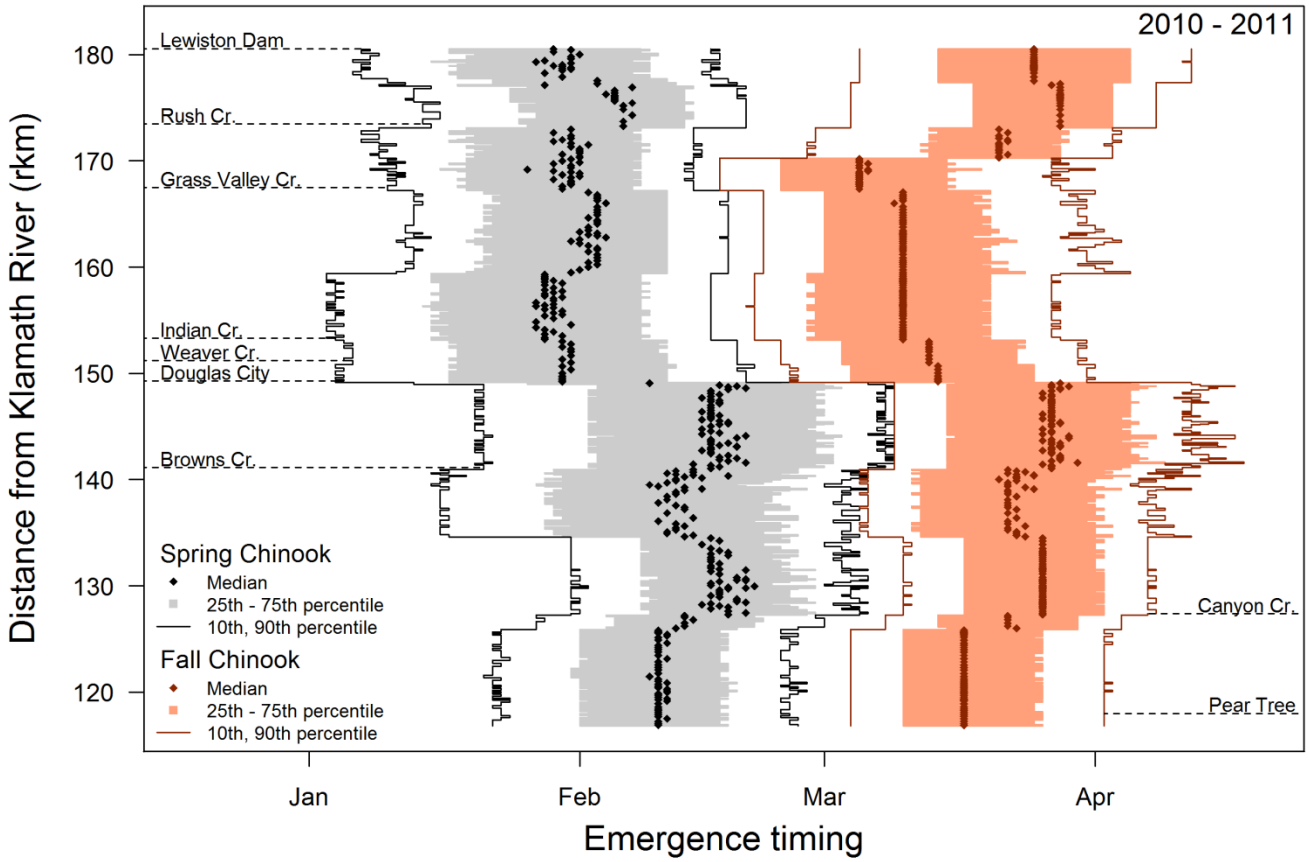

Figure 1-5. Graph showing the spatial and temporal distribution of natural-origin Spring and Fall Chinook Salmon fry emergence Reach simulated from empirical spawner survey data, Trinity River Restoration Reach, California, 2010–11. For each of the 356 meso-habitat units, thin lines (black and red) bound dates of the 10th and 90th percentiles of simulated fry emergence, horizontal bars (gray and orange) show the 25th–75th percentile range, and diamonds (black and red) show the median (i.e., the date when half of the fry population has emerged).

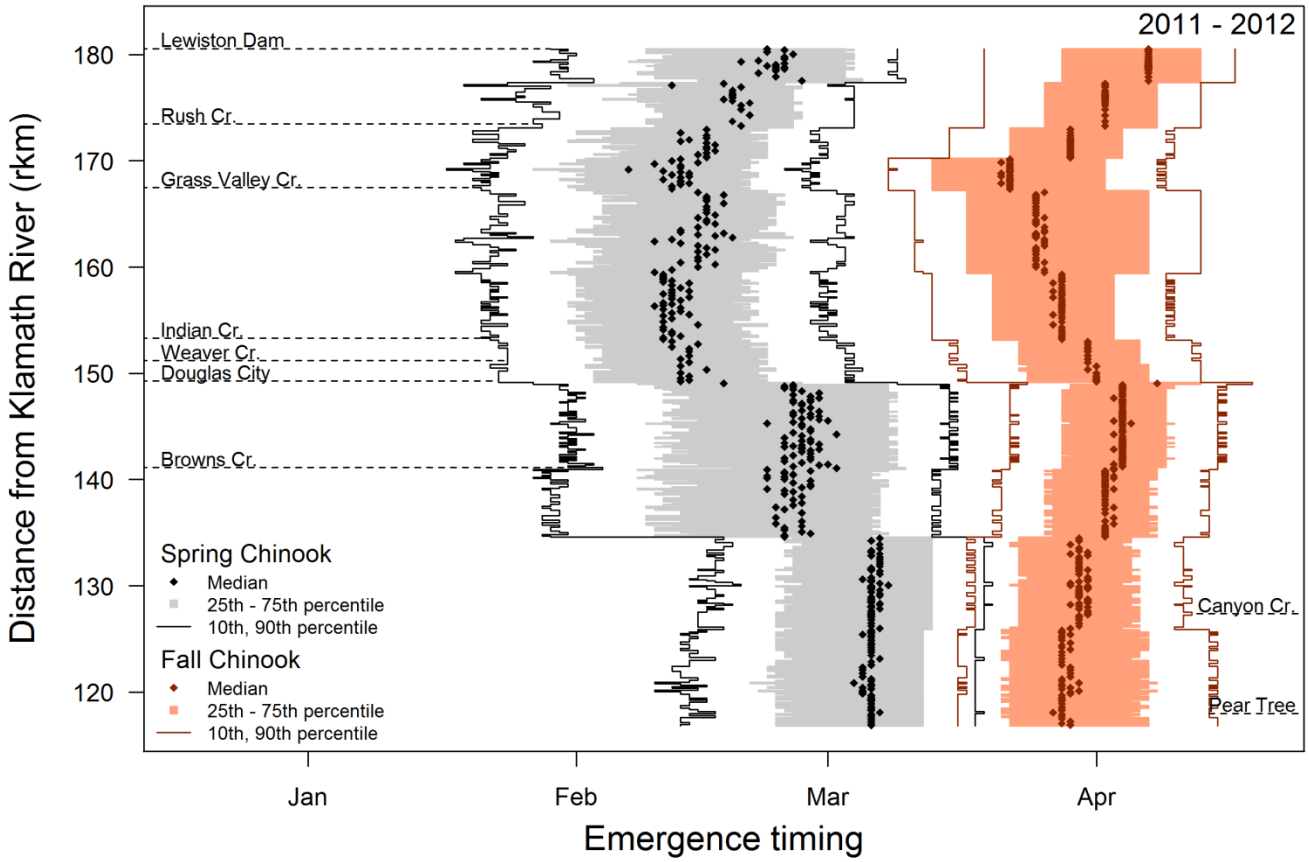

Figure 1-6. Graph showing the spatial and temporal distribution of natural-origin Spring and Fall Chinook Salmon fry emergence simulated from empirical spawner survey data, Trinity River Restoration Reach, California, 2011–12. For each of the 356 meso-habitat units, thin lines (black and red) bound dates of the 10th and 90th percentiles of simulated fry emergence, horizontal bars (gray and orange) show the 25th–75th percentile range, and diamonds (black and red) show the median (i.e., the date when half of the fry population has emerged).

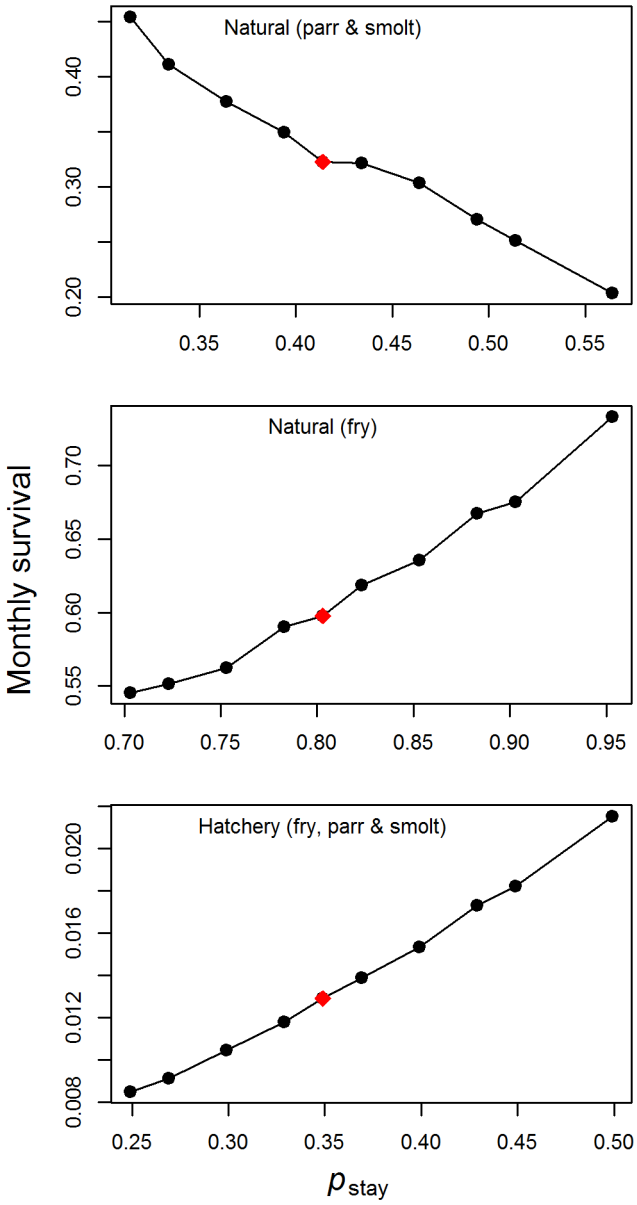

Figure 1-7. Graphs of sensitivity analysis results showing correlation between the movement model parameter p_{stay} and the calibrated survival parameter optimized to match weekly Pear Tree trap abundance estimates. Red diamonds show values of p_{stay} and survival when both parameters are estimated simultaneously by calibration. Black circles show estimated values of survival when calibrating the model from fixed values of p_{stay} that ranged from a -0.10 to 0.15 difference from the best-fit p_{stay} estimate. Monthly survival is calculated by raising the calibrated daily survival parameter to the power of 30.

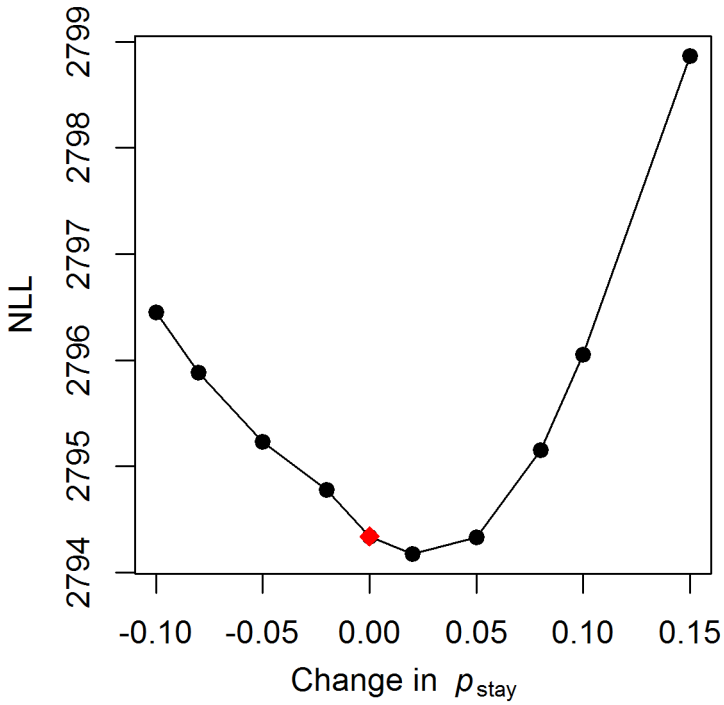

Figure 1-8. Graph showing negative log-likelihood (NLL) profile resulting from the sensitivity analysis undertaken to examine correlation between calibrated movement and survival parameters. The red diamond shows the NLL value of the model where p_{stay} and survival parameters were estimated jointly by calibrating to the weekly abundance estimates from Pear Tree trap. Black circles show NLL values for recalibrated models where survival was estimated when p_{stay} was fixed to values that ranged from -0.10 to 0.15 of the original calibrated p_{stay} value.

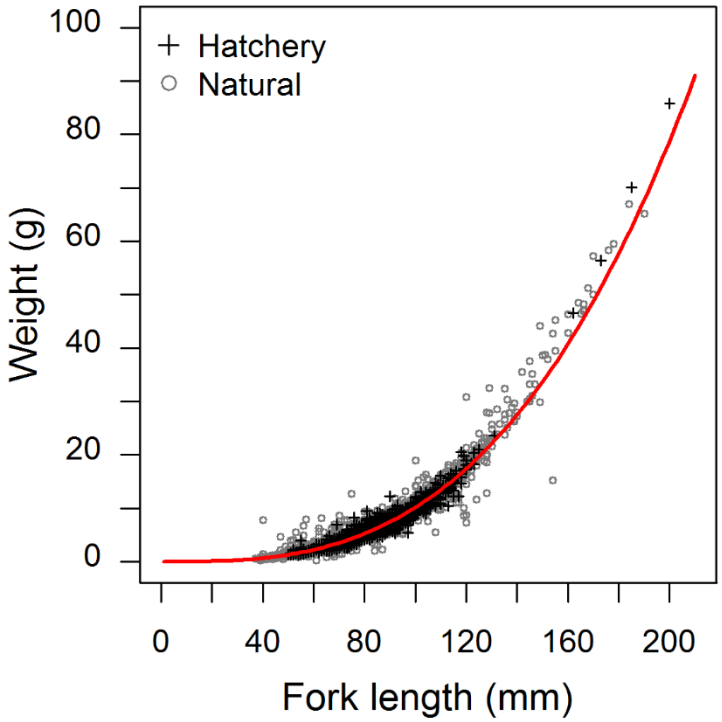

Figure 1-9. Scatter plot of hatchery and natural-origin Chinook Salmon fork-length and weight measurements observed at Pear Tree trap (n = 23,124), Trinity River, California. Samples were collected periodically during the outmigration period, January–August, 2006–2013. The red regression line ($W = 0.0000128L^{2.951}$, where W is mean fish weight in grams, and L is mean fork length in millimeters) is the length-weight relationship for simulated Chinook Salmon growth.

Publishing support provided by the U.S. Geological Survey
Science Publishing Network, Tacoma Publishing Service Center

For more information concerning the research in this report, contact the
Director, Western Fisheries Research Center
U.S. Geological Survey
6505 NE 65th Street
Seattle, Washington 98115
https://wfrc.usgs.gov/

ISSN 2331-1258 (online)
https://doi.org/10.3133/ofr20181174